

UNIVERSITY OF HELSINKI

REPORT SERIES IN PHYSICS

HU-P-D242

**INDIVIDUALIZED METHODS FOR PHYSIOLOGICALLY  
ADAPTED RADIATION THERAPY**

**Laura Tuomikoski**

Department of Physics  
Faculty of Science  
University of Helsinki  
Helsinki, Finland  
and  
HUCH Comprehensive Cancer Center  
Department of Radiation Oncology  
Helsinki University Central Hospital  
Helsinki, Finland

*ACADEMIC DISSERTATION*

*To be presented, with the permission of  
the Faculty of Science of the University of Helsinki,  
for public criticism in Auditorium of HUCH Comprehensive Cancer Center,  
Haartmaninkatu 4, 00290 Helsinki,  
on August 15<sup>th</sup>, 2016, at 12 o'clock noon.*

Helsinki, 2016

---

**Supervisors:**

Docent  
Mikko Tenhunen, Ph.D.  
Department of Radiation Oncology  
HUCH Comprehensive Cancer Center  
Helsinki, Finland

Docent  
Jani Keyriläinen, Ph.D.  
Department of Medical Physics  
Department of Oncology and Radiotherapy  
Turku University Hospital  
Turku, Finland

**Pre-examiners:**

Professor Dietmar Georg  
Div. Medical Radiation Physics  
Department of Radiation Oncology  
Medical University of Vienna  
AKH Wien, Austria

Professor Heikki Minn  
Department of Oncology and Radiotherapy  
Turku University Hospital  
Turku, Finland

**Opponent:**

Professor Eirik Malinen  
Department of Physics  
University of Oslo  
Oslo, Norway

Report Series in Physics HU-P-D242  
ISSN 0356-0961  
ISBN 978-951-51-2220-9 (printed version)  
ISBN 978-951-51-2221-6 (pdf version)  
<http://ethesis.helsinki.fi>

Unigrafia Oy  
Helsinki 2016

---

**L. Tuomikoski:** Individualized methods for physiologically adapted radiation therapy, University of Helsinki, 2016, 45 pages. University of Helsinki, Report Series in Physics; HU-P-D242

**Keywords:** Adaptive radiation therapy, risk-adapted radiation therapy, urinary bladder cancer, head and neck cancer

**Classification (INSPEC):** A8770H, B7510P, B7510R, B7520, B7520C

## Abstract

The rapid development of different imaging modalities related to radiation therapy (RT) has largely affected the entire RT process from the planning phase of the treatment to the final treatment delivery. Treatment planning requires accurate anatomical information that can be provided by computed tomography (CT) and magnetic resonance imaging (MRI). Additional functional information about tissues and organs can be obtained by functional MRI or nuclear medicine imaging techniques such as single-photon emission tomography or positron emission tomography. The introduction of cone-beam computed tomography (CBCT) imaging to the RT delivery process has also opened new possibilities for RT treatment. In the past, mainly bony anatomy was visualized with planar imaging, which was used for the localization of the treatment. With CBCT also the prevailing soft tissue anatomy in addition to bones can be verified on a daily basis. By taking advantage of the growing amount of information obtainable by imaging, RT treatment plans can be customized further to suit the individual anatomical and physiological properties of patients.

The focus of this thesis is on advanced methods for taking the individual variation in patients' physiology into account during the RT treatment planning. Two particular cases of variation are investigated: bladder filling and deformation during the RT of urinary bladder cancer, and radiation-induced changes of salivary gland function related to the RT of head and neck cancer. In both cases, pre-treatment imaging is used to create a patient-specific model to estimate the changes that would take place during the RT. The aim is to take these predicted changes into account in the treatment planning process, with the goal of protecting normal tissues.

At Helsinki University Central Hospital (HUCH), a method of adaptive radiation therapy (ART) was designed and clinically implemented for the treatment of urinary bladder cancer. In the applied workflow, four consecutive CT scans for RT treatment planning

---

were used to capture the changes in bladder shape and size while the bladder was filling. Assuming that a similar bladder filling pattern applies during the course of RT, four treatment plans corresponding to the different bladder volumes were prepared and stored in a plan library. Before each treatment fraction a CBCT scan was performed. The treatment plan, which was the closest match to the bladder shape and size of the day, was selected from the library and delivered accordingly. The use of ART enabled better conformity of the treatment. It considerably reduced the absorbed dose to the intestinal cavity, as compared to the non-adaptive approach. Furthermore, the dose coverage in the urinary bladder was not compromised, while the treatment margins were substantially reduced. Overall, the method was found to be feasible, and it was rapidly taken into clinical practice.

A model for predicting post-RT salivary flow was constructed and evaluated for the treatment of head and neck cancer. The model was based on pre-RT quantitative  $^{99m}\text{Tc}$ -pertechnetate scintigraphy, direct measurement of total salivary flow and population-based dose-response behaviour. A good correlation was found between the modelled and the measured values of saliva flow rate. Hence, the model can be used as a predictive tool for risk-adapted treatment planning. One possible explanation for the remaining discrepancies between the predicted and the measured saliva flow rate values may be patients' individual responses to radiation.

---

## Preface

This thesis is based on research projects conducted at HUCH Comprehensive Cancer Center, Helsinki University Central Hospital, between 2009 and 2015. Therefore, I would like to thank HUCH Cancer Center and its Director, Docent Petri Bono, for providing me with excellent research facilities and for the opportunity to work in the clinic.

I am most grateful to my supervisor, Docent Mikko Tenhunen, Chief Physicist and Head of Radiotherapy at HUCH Cancer Center, for his patient guidance in both research and clinical work. He has been a great source of inspiration and encouragement. He was always willing to offer me fresh ideas and words of wisdom, whenever I needed advice, a boost of confidence or just someone to talk to. I also want to thank my other supervisor, Docent Jani Keyriläinen, for his support during this process. He helped me realize that a PhD degree is just another milestone in the continuum of other, and sometimes even more important, life events.

I warmly acknowledge the previous and current heads of the doctoral program in Materials Research and Nanosciences (MATRENA) Prof. Kai Nordlund and Prof. Jyrki Räisänen, and the head of the Physics Department Prof. Hannu Koskinen from University of Helsinki for supporting my PhD studies. I am also grateful to Prof. Sauli Savolainen for guiding me through the studies and encouraging me towards the degree of a medical physicist. I thank the Finnish Cancer Foundation and Cancer Society of Finland, Finnish Society for Oncology, Emil Aaltonen Foundation, Ida Montin Foundation, Helsinki University Hospital and University of Helsinki for financial support over the years.

I express my gratitude to the official reviewers of this thesis, Prof. Dietmar Georg and Prof. Heikki Minn, for their constructive remarks, and for the pleasant co-operation and flexibility during the process. I am honoured to have Prof. Eirik Malinen as my opponent in the doctoral defence.

I also thank Donald Smart for revising the language of the thesis, and Heikki Karhiaho for providing the artwork for the printed cover.

During these years I have had the privilege of getting to know and to work with many wonderful people, who are truly devoted to the same cause - providing the best possible treatment for cancer patients. Special thanks go to all the people working at HUCH Cancer Center. I wish to thank all the co-authors, and I am especially grateful to Mika Kapanen and Juhani Collan for sharing their immense knowledge and incredible

---

enthusiasm towards radiotherapy and beyond. My warmest thanks go to physicists Tiina Seppälä, Juha Korhonen, Aino Valli, Anne Vestergaard and Ludvig Muren, as well as medical doctors Kauko Saarilahti, Harri Visapää, Venla Loimu and Jukka Sairanen, for the fruitful collaboration.

I have been privileged to have a support group of colleague physicist helping and encouraging me along this scientific journey. Heini Hyvönen, Satu Strengell, Toni Ihalainen and Antti Kulmala all deserve special thanks for their support and friendship. I would also like to thank Lea Hämäläinen, Jan Sarén and Timo Koponen, as without their presence in my life I would never even have graduated as a physicist.

The greatest joy in my life are my friends and family. I am most grateful to Taru and Riikka, my dear friends since childhood, for being there for me all these years. I want to thank my father Matti and my brother Jarkko for their love and support. In my heart I dedicate a part of this work to my mother Maritta, who would have been very proud to see this day.

There are no words to describe my gratitude towards my dear husband, Kirill. He has an amazing ability to find exactly the right words in every situation to help me keep going and to uncover some hidden strengths in me. He brings lots of love and happiness in my life. I am eagerly looking forward to the new exciting phase that is about to start in our life as a family.

Helsinki, July 2016

Laura Tuomikoski

---

## List of original articles

This thesis consists of an introductory part followed by four articles which are referred to by the Roman numerals **I – IV** throughout the text.

- I**            **Tuomikoski L**, Collan J, Keyriläinen J, Visapää H, Saarilahti K, Tenhunen M. Adaptive radiotherapy in muscle invasive urinary bladder cancer—an effective method to reduce the irradiated bowel volume. *Radiother Oncol* 2011;99:61-6.
- II**            **Tuomikoski L**, Korhonen J, Collan J, Keyriläinen J, Visapää H, Sairanen J, Saarilahti K, Tenhunen M. Implementation of adaptive radiation therapy for urinary bladder carcinoma: imaging, planning and image guidance. *Acta Oncol* 2013;52:1451-7.
- III**           **Tuomikoski L**, Valli A, Tenhunen M, Muren L, Vestergaard A. A comparison between two clinically applied plan library strategies in adaptive radiotherapy of bladder cancer. *Radiother Oncol* 2015;117:448-52.
- IV**            **Tuomikoski L**, Kapanen M, Collan J, Keyriläinen J, Saarilahti K, Loimu V, Seppälä T, Tenhunen M. Toward a more patient-specific model of post-radiotherapy saliva secretion for head and neck cancer patients. *Acta Oncol* 2015;54:1310-6.

Articles I and III are reprinted with the kind permission of Elsevier, Copyright © 2011 and 2015 Elsevier Ireland Ltd. Articles II and IV are reprinted with the permission of Taylor & Francis, Copyright © 2013 and 2015 Informa Healthcare.

---

## Author's contribution

**Study I:** *“Adaptive radiotherapy in muscle invasive urinary bladder cancer—an effective method to reduce the irradiated bowel volume”*

In this publication we reported the ART protocol for urinary bladder cancer developed and applied at HUCH. The emphasis on this work was placed on determining normal tissue doses and dose coverage in the bladder. The author participated in the planning of the research, collected and analysed the data, and was responsible for preparing the manuscript.

**Study II:** *“Implementation of adaptive radiation therapy for urinary bladder carcinoma: imaging, planning and image guidance”*

In this article the expansion of urinary bladder dimensions during treatment was investigated. In addition, partial bladder treatment was evaluated and a procedure for reducing CBCT imaging dose was introduced. The author participated in the planning of the study and undertook the majority of the data collection and analysis. The author took an active part in writing the article.

**Study III:** *“A comparison between two clinically applied plan library strategies in adaptive radiotherapy of bladder cancer”*

This article compared two clinically applied plan-library-based approaches to bladder ART. The author took part and supervised the planning of the study and developing and performing the data analysis, and was responsible for writing the article.

**Study IV:** *“Toward a more patient-specific model of post-radiotherapy saliva secretion for head and neck cancer patients”*

In this research post-RT salivary flow was modelled for head and neck cancer patients. The author participated in the planning and the research and data analysis. The publication was written by the author of this thesis.



---

## Symbols and abbreviations

AP	anterior-posterior
ART	adaptive radiation therapy
AUH	Aarhus University Hospital
CBCT	cone-beam computed tomography
CC	cranial-caudal
CT	computed tomography
CTV	clinical target volume
$D_{mean}$	mean absorbed dose
$D_{50}$	the absorbed dose causing a 50-% reduction in salivary gland excretion fraction
DVH	dose-volume histogram
GTV	gross tumour volume
HUCH	Helsinki University Central Hospital
IC	intestinal cavity
IMRT	intensity-modulated radiation therapy
$k$	fitting parameter for the sigmoidal dose-response function
linac	linear accelerator
LR	left-right
MRI	magnetic resonance imaging
NM	nuclear medicine
OAR	organ at risk
PET	positron emission tomography
PTV	planning target volume
QA	quality assurance
rEF	relative excretion/ejection fraction
ROI	region of interest
RT	radiation therapy
SD	standard deviation
sEF	salivary gland excretion/ejection fraction
SPECT	single-photon emission computed tomography
VMAT	volumetric-modulated arc therapy
2D	two-dimensional
3D	three-dimensional

---

## Contents

<b>1</b>	<b>Introduction</b>	<b>1</b>
1.1	The role of medical imaging in the individualization of RT process	1
1.2	Adaptive RT	2
1.3	Risk-adapted RT	7
<b>2</b>	<b>Aims of the thesis</b>	<b>8</b>
<b>3</b>	<b>Materials and methods</b>	<b>9</b>
3.1	Modeling of organ motion/physiological changes for ART of urinary bladder cancer	9
3.1.1	The workflow for online-ART of urinary bladder cancer at HUCH	9
3.1.2	Modeling inter- and intra-fractional changes in the urinary bladder	11
3.1.3	Evaluation of normal tissue irradiation and target coverage in ART of urinary bladder cancer	12
3.2	Modeling of salivary gland function for risk-adapted RT of head and neck cancers	13
3.2.1	Construction of the individual salivary flow model	15
3.2.2	Evaluation of patient-specific variation in salivary gland scintigraphy	16
<b>4</b>	<b>Results</b>	<b>18</b>
4.1	Managing organ motion/physiological changes in ART of urinary bladder cancer	18
4.1.1	Time trends in urinary bladder volume	18
4.1.2	The benefits of ART for urinary bladder cancer	22
4.2	Predicting salivary gland function in risk-adapted RT of head and neck cancers	25
4.2.1	Individual salivary flow model	25
4.2.2	Patient-specific variation in salivary gland scintigraphy	27
<b>5</b>	<b>Discussion</b>	<b>29</b>
5.1	Changes of bladder dimensions between and during RT treatment fractions	29
5.2	ART workflow for urinary bladder cancer implemented at HUCH	30
5.3	Prediction of salivary flow after RT of head and neck region	32
<b>6</b>	<b>Conclusions</b>	<b>36</b>
	<b>References</b>	<b>37</b>

# 1 Introduction

## *1.1 The role of medical imaging in the individualization of RT process*

Traditionally, the external beam radiation therapy (RT) process has been seen as a fairly rigid and predictable chain of standard procedures. This process consists of

- 1) medical imaging with a carefully fixed patient position, providing three-dimensional (3D) anatomical information of the target volume, organs at risk (OARs) and surrounding tissues,
- 2) treatment planning including segmentation of the volumes of interest in the treatment planning images, selection of the RT technique, planning of treatment field set-up and calculation of the corresponding radiation dose distribution and
- 3) treatment delivery typically carried out with a linear accelerator (linac) in a series of successive treatment fractions.

During the last decades, medical imaging has vastly increased its importance in the process of RT treatment planning and delivery. Computed tomography (CT), magnetic resonance (MR) or nuclear medicine (NM) imaging can be applied to characterize the individual patient anatomy and physiology [1]. CT and MR imaging are used to obtain 3D anatomical information for the RT workflow. Functional MR and NM imaging, including positron emission tomography (PET), single-photon emission computed tomography (SPECT) and planar scintigraphy, can provide additional functional information of the target volume and normal tissues to be used in treatment planning. Dose calculations are usually based on the anatomy and heterogeneous tissue electron density information of a CT image [1]. In the treatment delivery, imaging is applied for ensuring the proper localization of the RT treatment. Modern linacs are equipped with an integrated X-ray imaging device, which can be utilized either for two-dimensional (2D) planar imaging or 3D cone-beam computed tomography (CBCT). The 2D imaging superimposes underlying anatomical structures of medical interest. Therefore, quite often mainly the bony anatomy can be visualized, and the patient position and localization of the treatment is verified and corrected based on the bones. In contrast, the other on-board solution, 3D CBCT, overcomes this technical aspect. In addition to bony structures, CBCT is able to visualize soft tissue anatomy. This is a major advantage when treating soft tissue tumours, such as pelvic tumours. Volumetric data can be used to detect changes and deformation in tissues and organs during the course of RT, thus sometimes revealing

## INTRODUCTION

---

for example the need for the re-planning of the treatment.

As anatomical and physiological features may vary substantially between individual patients, the RT is planned using population-based knowledge of the properties of an average patient. The basis of this knowledge lies in the mixture of previous research reported in the literature and the clinical experience gained at the department. Treatment planning is based on the individual anatomical information captured at the instant of planning CT imaging. However, many assumptions and generalizations are usually made about the geometry and dynamics of a volume to be treated, the effectiveness of treatment and the probability of radiation-induced side-effects. Anatomical variations, including organ motion and deformation of both tumour and normal tissues, complicate RT treatment. The treated volume should be large enough to accommodate most variations seen in individual patients, but on the other hand it should be as small as possible to minimize treatment toxicity. The historical approach is to measure the variations for a certain treatment site in a large population, and calculate how much the treated volume needs to be expanded beyond the tumour to be able to cover most variations. Several techniques for deriving a suitable safety margin have been reported in the literature [2-6]. A safety margin may be designed based on the probability of the correct target dosage, for example to ensure a 95% minimum dose in target volume for 90% of patients [4]. A corresponding standard treatment margin is then applied for all patients regardless of whether they show large variations or not. A similar convention applies for the definition of the prescribed doses. The goal is to give the dose enabling maximum probability of cure without complications, which is once again defined in a population. However, in reality, a patient may crucially differ from the average patient, thus introducing uncertainty in the treatment delivery and the prediction of the treatment outcome.

The growing selection of different imaging techniques provide important tools for customizing treatments to the needs of an individual patient. More accurate, patient-specific anatomical and physiological information may help reducing the overall uncertainty in the RT process. This may enable dose escalation in the tumour and/or reduce treatment toxicity by improved shielding of the OARs.

### *1.2 Adaptive RT*

In adaptive radiation therapy (ART) the traditional chain of events along the RT process is usually broken to achieve highly individualized treatment. The concept was introduced in the literature by Di Yan *et al.* [7]. Their article defined ART as a closed loop of the RT

process, where systematic feedback of the individual patient variations is used to modify the treatment plan. During the process variations are systematically monitored and incorporated via re-optimization of the treatment plan [7]. This method provides a possibility to tailor treatment margins to specific patients and/or alter treatment doses to enable safe dose escalation.

Soft tissue tumours in the pelvic area are particularly suitable for ART, as the pelvic region is subject to continuous changes driven by physiological activity [8]. Bowel movement and rectal and bladder filling cause organ motion and deformations in the pelvic region [9]. Thus, the prostate, urinary bladder, rectum and cervix are mobile targets for RT, and organ deformation can be a major problem for these tumour sites [10-15]. Hence, it is not surprising that many of the first clinical implementations of ART techniques were particularly reported for pelvic tumours [8,16-18].

Fundamentally, there are three different scenarios for applying treatment plan modifications. In the first approach, the treatment plan can be altered off-line, based on a pre-defined triggering criteria or at a certain temporal point during the treatment course (offline ART) [16,18-23]. In this scenario, anatomic variations can be observed and measured during the initial treatment fractions using e.g. CBCT imaging. This information may then be used to construct a new target volume for re-planning the treatment, or if large deformations were detected, it could trigger a new treatment planning CT. In the offline ART method, the original treatment plan is replaced by a new, modified treatment plan, which aims at incorporating the anatomical variations seen during the previous treatment fractions. The other two approaches aim at quantifying the individual variations before each treatment fraction, and immediately adapting the treatment to the current anatomy (online ART). In the second adaptive method, several alternative treatment plans are prepared and stored in a so-called plan library [24-26]. The decision of the treatment plan selection is made on-line on a daily basis. Usually based on pre-treatment CBCT imaging, the anatomy of interest is determined each day, and the treatment plan that has the best correspondence to the current anatomy is selected. The third option is to modify the treatment plan on-line by either full re-optimization of the dose distribution or e.g. beam aperture modification. In this approach, usually volumetric imaging is used to define the anatomic situation before the treatment, and immediate actions are taken, while the patient lies on the treatment table, to adjust the original treatment plan to fit the current anatomy. The challenge of the on-line re-optimization method is that it requires a smooth and a rapid workflow including a reliable deformable registration and fast re-optimization and dose accumulation. It also requires special expertise of the personnel responsible for treatment delivery. Hence, this method is not

## INTRODUCTION

---

easily introduced into a clinical routine, although a pioneering clinical implementation in MRI-based on-line re-optimization was introduced very recently [27].

### **ART for urinary bladder cancer**

In 2014, urinary bladder cancer was the fourth common cancer in men, representing 5.7% of all male cancers in Finland, being more common in male than in female population (appearance of 15.4 vs 3.7/100.000) [28]. Urinary bladder is a hollow organ consisting of epithelium, connective tissue and several muscular layers [29]. The choice of the cancer treatment is dependent on whether the tumour has invaded into the muscular layers in the bladder wall or continues to spread to adjacent organs [29,30]. In Finland, the standard treatment for localized muscle-invasive bladder carcinoma is a surgical resection of the whole bladder (radical cystectomy). However, an alternative treatment enabling organ preservation is RT, which is often preceded by transurethral resection of the bladder tumour and combined with chemotherapy [29,31,32]. This option may be offered for patients with inoperable tumours or who are unfit for cystectomy (e.g. elderly patients). Urinary bladder is a challenging target for RT. The filling of the bladder varies, hence affecting the treatment volume. In addition, there are daily variations of shape and position of the bladder caused by rectal filling or bowel loops adjacent to the bladder. Previously, this problem has been solved by adding large treatment margins, usually within the range of 15-20 mm, around the bladder [33-36], consequently resulting in large irradiated volumes of normal tissue.

In RT of urinary bladder cancer, the first ART applications involved controlled offline re-planning. In a study reported in 1993 [37], which can be considered as an early clinical application of a very simple bladder ART workflow, all patients had a second CT scan half way through their treatment. The changes in the target volume and adequacy of the original treatment plan were assessed, and a new treatment plan was created if found necessary. The following contributions to the literature in clinically applied bladder ART introduced more sophisticated ART workflows. The first studies addressed offline ART strategies [18,20], while later a shift towards the online ART approaches was seen.

At present, the dominating ART strategy for bladder cancer is based on the use of pre-calculated treatment plan libraries. To quantify variations in bladder shape, size and position for generating the plan library, mainly two approaches have been applied. The first method, which is presented in this thesis and currently used at Helsinki University Central Hospital (HUCH), aims at capturing different bladder volumes from an empty to a full bladder by multiple successive planning CT scans. An individual treatment plan is

calculated for each filling state of the bladder and stored in a plan library. This kind of method can also be based on merely two CT acquisitions, one with an empty and another with a full bladder, by using interpolation tools or varying margin expansions [25,38,39]. The idea behind this method is to provide a solution for varying bladder filling, while also allowing some bladder deformation. In the second approach, the treatment is initiated as a conventional RT, and deformation and positional changes of an empty bladder are monitored using the CBCT images acquired during the first treatment fractions [24,40]. Here, the variations in the shape and position of the empty bladder are incorporated by combining the information from daily CBCTs into the adaptive target volumes. Based on these volumes, a treatment plan library is created and applied for the remaining treatment fractions. Another method suggested for plan library creation is expanding the bladder volume in a single treatment planning CT by several different margins [35,41]. However, this technique does not provide any information on the individual, patient-specific patterns of bladder expansion.

The different clinically implemented plan-library-based ART workflows for bladder cancer are listed in Table 1-1, following the chronological order of appearance in the literature. Simulation studies of online re-optimization for bladder ART have been performed [42,43], but so far no clinical implementations have been reported.

A large part of this thesis concentrates on accounting for the changes in the urinary bladder during the treatment course. The plan-library-based protocol for urinary bladder ART implemented at HUCH will be presented and evaluated. The suggested workflow will also be compared to another plan-library-based ART protocol that has been clinically applied in Aarhus University Hospital (AUH), Denmark [40].

## INTRODUCTION

---

*Table 1-1. The different clinically implemented plan-library-based ART workflows for bladder cancer introduced in the literature.*

<b>Study</b>	<b>Site</b>	<b>Treatment plan library</b>
Foroudi <i>et al</i> , 2011, [24]	Peter MacCallum Cancer Centre, Melbourne	Three plans created from a composite of one planning CT and five CBCTs
Murthy <i>et al</i> , 2011, [41]	Tata Memorial Centre, Mumbai	Six plans created from planning CT by varying CTV-to-PTV margin
Tuomikoski <i>et al</i> , 2011, [Study I]	Helsinki University Central Hospital, Helsinki	Four plans created from four planning CTs
Meijer <i>et al</i> , 2012, [25]	Catharina Hospital Eindhoven, Eindhoven	Six plans created from two planning CTs by using inter- and extrapolation
McDonald <i>et al</i> , 2013, [38]	The Royal Marsden Hospital, Sutton	Three plans created from two planning CTs by varying CTV-to- PTV margin
Vestergaard <i>et al</i> , 2014, [40]	Aarhus University Hospital, Aarhus and Copenhagen University Hospital, Herlev	Three plans created from a composite of one planning CT and four CBCTs



### 1.3 Risk-adapted RT

In addition to anatomic variations, ART can be applied to compensate for the radiation sensitivity of normal tissues or tumour. The latter option was also implied by Yan *et al*: “the concept of ART can also be applied to compensate for other treatment variations such as radiation sensitivity and density of clonogenic cells when they become measurable during the treatment course” [7]. There are a few examples of risk-adaptive RT in the literature. To meet the criteria for the definition of ART, some indicator of the radiation sensitivity of tissues of interest should be measured during the course of RT and trigger treatment plan adaptation. There are many examples of procedures applied for determining tumour response or normal tissue function during RT using functional imaging [44,45]. Some of these methods have been suggested as predictive tools for treatment outcome [46-48], and they could even be used as a basis for individualized treatment plan modifications [49-54]. The intended modifications aim at dose escalation to a radioresistant tumour or parts of the tumour, boosting a shrinking tumour or sparing normal tissues. However, adapting treatment to the individual biology of the tumour or normal tissues may be problematic due to different uncertainties related to functional imaging [55,56].

One possibility of adapting RT based on the potential risks caused to the patient is the use of different predictive models as a tool for treatment planning. In this case, the risk of producing a certain side-effect for the given treatment is evaluated, and the treatment plan or the prescribed dose can be adjusted based on this risk evaluation [49,52,57,58]. Here, the risk evaluation and the required treatment modifications usually take place before the initiation of RT treatment.

One example of the modelling of radiation-induced normal tissue effects is the prediction of salivary gland function related to RT of head and neck cancers. These models require the use of pre-treatment functional measurement to determine the initial activity of the salivary glands. Several methods have been reported in the attempt of quantifying salivary gland function for this purpose. The applied techniques include direct measurements of secreted saliva volume, functional MRI, PET, SPECT and scintigraphy [59-65].

The latter part of this thesis addresses the prediction of post-RT salivary gland function. A predictive model, to be later used for risk-adapted treatment planning for RT of head and neck cancers, is introduced and evaluated.

## 2 Aims of the thesis

This thesis aimed to establish clinically feasible methods of predicting physiology-driven changes on the individual patient level, and to incorporate these changes into RT treatment planning. Patients with two different types of cancer were involved in this study: urinary bladder cancer and head and neck cancers. In both patient populations methods of responding to the individual physiology were developed with the goal of reducing the absorbed dose to the normal tissues.

The specific aims were:

1. to quantify changes in the shape and size of the urinary bladder taking place during and between RT treatment fractions (Studies I and II),
2. to design and clinically implement a workflow for ART of urinary bladder cancer, to compare this workflow with the conventional, non-adaptive approach, and also with another clinically used ART workflow (Studies I and III), and
3. to quantify and predict RT-induced changes in salivary gland function, and to assess inter-patient differences in post-RT salivary gland function (Study IV).

### 3 Materials and methods

#### *3.1 Modeling of organ motion/physiological changes for ART of urinary bladder cancer*

At HUCH, an ART strategy for urinary bladder cancer was designed and clinically implemented in 2009. The motivation behind the new treatment technique was to reduce the treatment margins in order to minimize the irradiated normal tissue volume that could potentially affect treatment toxicity. The ART protocol at HUCH has evolved over the years, hence the current workflow is described in the following.

##### *3.1.1 The workflow for online-ART of urinary bladder cancer at HUCH*

In the HUCH protocol, the prediction of changes in bladder volume and shape is based on repeated planning CT imaging. The different states of bladder filling are captured by a sequence of four repeated CT scans acquired at 15-minute intervals. Right before the first scan ( $t=0$ ) the patients empty their bladders and drink 8 dl of water. For all four CTs with different bladder volumes a set of contours is generated including clinical target volumes (CTV), planning target volumes (PTV), bladder (if not equal to CTV), rectum and intestinal cavity (IC). These structures are copied into the first planning CT with an empty bladder, which is used for treatment plan calculations. A library of four treatment plans, one plan for each PTV, is generated using volumetric-modulated arc therapy (VMAT) or intensity-modulated radiation therapy (IMRT). Sometimes bladder filling during the planning CT sequence is found to be modest, and then individual decisions of excluding one or even two of the treatment plans for the middle-sized PTVs can be made.

On each day of treatment, patients empty their bladder before being positioned on the treatment couch, and a daily CBCT image is acquired. A soft tissue match is used between the CBCT and treatment planning CT, containing contours of all four bladders of different sizes and PTVs. The 3D registration is performed by centring the bladder visible in the CBCT image inside the smallest bladder contour encompassing the entire bladder, and then the corresponding treatment plan is selected from the library and the treatment is delivered. If the lymph node region is treated, then a registration based on bony structures is used. No instructions about the fluid intake are given to the patients during the course of treatment. A simple description of the treatment workflow is illustrated in Figure 3-1.

## MATERIALS AND METHODS

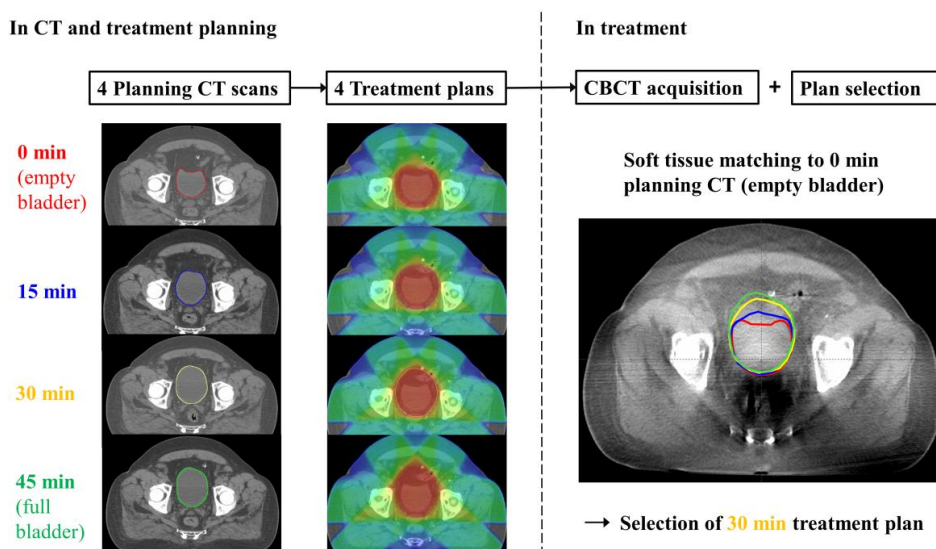


Figure 3-1. The workflow of the ART for bladder cancer according to the protocol applied at HUCH.

### Patients and PTV definitions

Altogether 18 patients with muscle-invasive T2–T4a urinary bladder cancer considered unfit for cystectomy were included in Studies I–III. No informed consent was obtained from the patients, as all these studies were designed to retrospectively evaluate the currently applied treatment technique. The patients received ART for bladder cancer at HUCH between 2009 and 2014. For 10 patients, Lipiodol contrast agent was injected into the bladder wall during cystoscopy to mark the gross tumour volume (GTV) [66,67]. The prescribed radiation dose varied according to the treatment volume. In the elective treatment phase the patients received ART for the whole bladder with or without lymph node irradiation up to 44–50.4 Gy with a fraction size of 1.8 or 2 Gy. CTV-to-PTV margins of 10 mm in the anterior and cranial directions and 15 mm in other directions were applied for the bladder. An isotropic margin of 7 mm was added around the lymph node region, if they were treated. A partial bladder boost treatment of 10–20 Gy was delivered using a CTV-to-PTV margin of 10 mm. Three patients received a partial bladder treatment of 52.5 Gy/2.5 Gy due to impaired bladder function and several co-morbidities.

### 3.1.2 Modeling inter- and intra-fractional changes in the urinary bladder

For the analysis of time trends in bladder volumes throughout the treatment course, daily bladder volumes were contoured in the CBCT images for the patients included in Studies I and III. In Study II, intra-fractional volumetric changes were modelled using the bladder contours in the successive planning CT images. For these patients, an additional post-treatment CBCT image was acquired at least on a weekly basis to enable evaluation of intra-fractional bladder filling rate.

To estimate the changes of bladder size, a simple ellipsoidal model was applied, using the maximal dimensions of bladder in the cranial-caudal (CC,  $z$ ), anterior-posterior (AP,  $y$ ) and left-right (LR,  $x$ ) directions, measured from the planning CT scans. The anatomical points of origin, relative to which the measurements were performed, were the most caudal point in the empty bladder wall (CC direction), the most posterior point in the empty bladder wall (AP direction) and the midline of symphysis (LR direction). In the ellipsoidal model the bladder volume  $V$  was calculated as

$$V = \frac{4\pi}{3} \cdot \frac{z_{cran} + z_{caud}}{2} \cdot \frac{y_{ant} + y_{post}}{2} \cdot \frac{x_{left} + x_{right}}{2}, \quad (1)$$

where the dimensions  $z$ ,  $y$  and  $x$  were measured relative to the anatomical origin.

To investigate the maximum displacements of the bladder wall during a typical treatment fraction of 15 minutes, an assumption was made that all bladder growth is manifested only in one dimension, while the other two orthogonal dimensions remain constant. A theoretical limit for the maximum change  $\Delta z$  (or  $x$ ,  $y$ ) in the direction of dimension growth, caused by the volume change  $\Delta V$ , can be formulated by differentiating Eq. (1) partially with respect to  $z$ , while  $x$  and  $y$  are constant:

$$\frac{dV}{dz} = \frac{4\pi}{3} xy. \quad (2)$$

Dividing Eq. (2) by  $V$  and substituting  $V = \frac{4\pi}{3} zyx$  gives the rate of the change in bladder dimension as a function of volume,

$$\frac{\Delta z}{\Delta V} = \frac{z}{V}, \quad (3)$$

which shows that as the volume  $V$  increases, the rate of the change of bladder size decreases. Alternatively, if the bladder expansion is assumed to be isotropic in all

## MATERIALS AND METHODS

---

directions ( $\Delta z \approx \Delta x \approx \Delta y$ ), the wall displacement is 1/3 of the maximum change given by Eq. (3),

$$\frac{\Delta z}{\Delta V} = \frac{1}{3} \frac{z}{V}. \quad (4)$$

The elliptical bladder model and the worst case scenario of intra-fractional bladder dimension growth were compared with the actual bladder volume and changes in bladder wall extreme positions in planning CT scans in Study II.

### *3.1.3 Evaluation of normal tissue irradiation and target coverage in ART of urinary bladder cancer*

In Studies I and III, the benefits of ART strategy for urinary bladder cancer were evaluated. For this purpose, bladder and IC contours were segmented in the daily CBCT images in Study I. Dose to the IC and dose coverage in the bladder were estimated for the ART technique, as compared to the conventional non-ART protocol. Daily IC and bladder contours were copied from CBCT images into treatment planning CT images, by applying the online image registration of each treatment fraction. Three different dose-volume histogram (DVH) curves were calculated for each of the IC volumes using the treatment planning CT images. One DVH was calculated using the daily ART plan, and the other two DVHs from the non-ART plans using both isotropic and anisotropic CTV-to-PTV margins. The total cumulative DVHs for the IC volumes were calculated from the daily cumulative DVHs with the numerical computing software Matlab version 7.8 (MathWorks Inc., Natick, MA, USA), by summing up the absolute doses in bins of 5 cm<sup>3</sup> absolute volume. This direct summation of DVHs produces the “worst case” scenario, where the same IC element is constantly at the point of the highest dose. Additionally, dose coverage in the bladder was evaluated by recording the minimum doses in the bladder for each treatment fraction.

### **Comparison of two adaptive strategies**

In Study III, the strategy of plan library creation applied at HUCH (so-called RepeatCT) was compared to a different strategy (so-called RepeatCBCT), which was clinically applied at AUH. In the RepeatCBCT method one planning CT with an empty bladder and four CBCT images acquired during the first week of treatment were contoured, and the bladder contours were combined using Boolean operators to form two adaptive composite PTVs. In addition, a non-adaptive PTV was generated by applying generous, population-

based margins around the empty bladder in the planning CT, resulting in a library of three different treatment plans. The investigated workflows were slightly modified from the original, clinically applied workflows by applying identical image registration procedure and CTV-to-PTV margins for both methods, hence enabling a straightforward comparison between two methods of generating adaptive PTVs. The margins used in the creation of different PTVs can be found in Study III.

### *3.2 Modeling of salivary gland function for risk-adapted RT of head and neck cancers*

In Study IV, a model for predicting the loss of salivary gland function after RT for head and neck cancers was developed and evaluated. The clinical aim was to provide a tool for treatment planning on an individual patient level, for guiding the decision of which salivary glands should be spared and to what extent, based on the predicted risk of salivary flow degradation.

#### **Patients and measurements**

The study population consisted of 70 head and neck cancer patients who received RT at HUCH during the years of 2006–2008 (50 patients) and 2012–2013 (20 patients). An informed consent was obtained from these patients. All the patients were treated bilaterally using thermoplastic mask fixation to the total dose of 50–70 Gy (fractional dose 2 Gy), by using an IMRT technique with 6 MV photons. Portal imaging was used for verifying patient positioning. Six patients were excluded from the salivary flow model due to incomplete sets of measurements.

For the salivary flow model, measurements of both the total volume of the produced saliva and relative input from each individual salivary gland to the total saliva output were required. Direct measurement of total salivary flow and salivary gland scintigraphy were performed before RT (70 patients), 6 months after RT (70 patients) and 12 months after RT (50 patients). The rate of the saliva production under oral stimulation was measured by collecting saliva in a measuring glass for 15 minutes, when patient was chewing a piece of paraffin wax. In scintigraphy, the excretion fractions of individual salivary glands were quantified by 30-min dynamic imaging with a gamma camera in 30-s time frames beginning simultaneously with an intravenous injection of  $^{99m}\text{Tc}$ -pertechnetate. After the first 15 minutes, 10 ml of 25% lemon juice solution was given orally to the patient to stimulate the saliva excretion. A typical scintigraphy curve is presented in Figure 3-2.

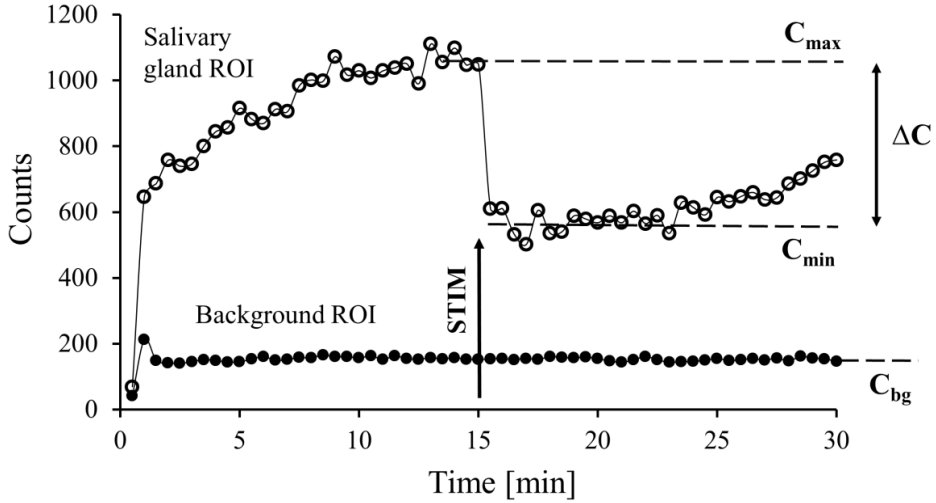


Figure 3-2. The number of detected counts in a dynamic scintigraphy image for the salivary gland's region of interest (ROI) and background ROI. The number of counts before ( $C_{max}$ ) and after ( $C_{min}$ ) the lemon juice stimulus are calculated as an average of four successive image frames. Each image in the dynamic series is acquired within 30 s, and the stimulus is applied at  $t = 15$  min.

The detected counts as a function of time were plotted for five regions of interest (ROI), one for each major salivary gland and one for the background. Using the number of counts inside the salivary gland ROI right before ( $C_{max}$ ) and after ( $C_{min}$ ) the lemon juice stimulus, the salivary excretion fraction sEF was calculated separately for all four glands using the equation

$$sEF = \frac{C_{max} - C_{min}}{C_{max} - C_{bg}}, \quad (5)$$

where  $C_{bg}$  is the number of counts in background ROI, normalized to the salivary gland ROI area. The relative excretion fraction at time  $t$  after RT was calculated by equation

$$rEF(t) = \frac{sEF(t)}{sEF(0)}, \quad (6)$$

where  $sEF(0)$  is the baseline value measured before RT.



3.2.1 Construction of the individual salivary flow model

The salivary flow model used in Study IV was based on the model reported in the previous work of Tenhunen *et al.* [68]. In this model, the relative total salivary flow under stimulation was calculated from a weighted sum of the expected relative excretion fractions for all functioning major salivary glands. In Study IV, the idea is developed further by using the absolute values of saliva flow rate by adding the parameter of pre-RT saliva flow rate in the model. The required input parameters for the new model are summarized in Figure 3-3.

The weighting coefficients for individual glands were derived by assuming that the volume of saliva secreted by a single gland in response to the stimulation is directly proportional to the count difference in ROI before and after stimulation,  $\Delta C_i = (C_{max} - C_{min})_i$ . Thus, the proportion of single gland saliva output  $m$  of the total saliva production could be expressed by the equation

$$m_i = \frac{\Delta C_i}{\sum_j \Delta C_j}, \quad (7)$$

where  $\sum_j \Delta C_j$  is the sum over all functioning major salivary glands.

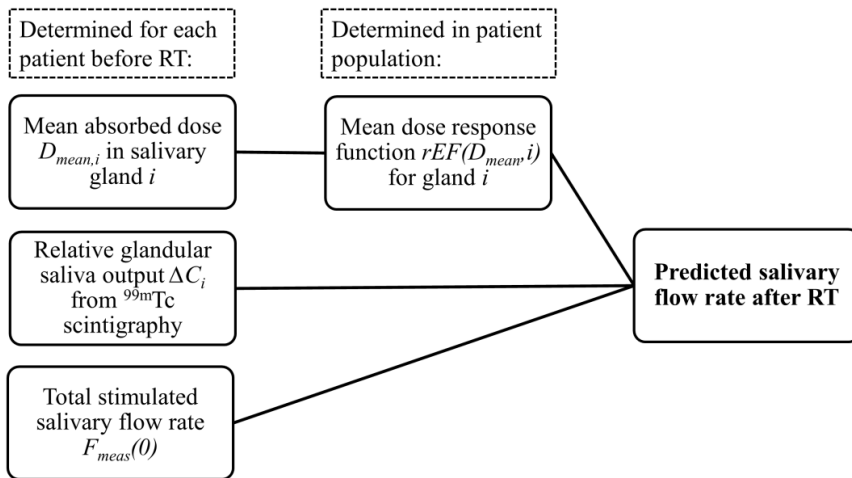


Figure 3-3. The input parameters needed for the salivary flow model in the prediction of post-RT salivary flow rate for an individual patient.

## MATERIALS AND METHODS

---

The dose-response relationship for rEF was assumed to have the shape of a sigmoidal function described by the equation

$$rEF = 1/[1 + \left(\frac{D_{mean}}{D_{50}}\right)^k], \quad (8)$$

where  $D_{mean}$  is the mean glandular dose,  $D_{50}$  is the dose for a 50% reduction in sEF and  $k$  represents the steepness of the curve. For further analysis, parameters  $D_{50}$  and  $k$  were determined by a nonlinear fitting in Matlab software. However, in the construction of the salivary flow model previously reported values of  $D_{50}$  and  $k$  were applied [68].

The total stimulated salivary flow  $F_{calc}(t)$  at time  $t$  after RT was calculated by applying Eqs 7 and 8 in the following expression

$$F_{calc}(t) = F_{meas}(0) \cdot \sum_i m_i \cdot rEF(D_{mean,i}). \quad (9)$$

Here  $F_{meas}(0)$  is the total stimulated saliva flow rate measured before RT, and  $m_i$  and  $rEF(D_{mean,i})$  are the proportion of single salivary gland  $i$  output of the total saliva output and the mean dose-response for gland  $i$ , respectively. In this model only the saliva production of the parotid and the submandibular glands are included, thus ignoring the excretion from the sublingual and the minor salivary glands.

### 3.2.2 Evaluation of patient-specific variation in salivary gland scintigraphy

A great inter-patient variance has been reported for salivary gland function measured at HUCH as well as elsewhere [69,70]. In Study IV, the scintigraphy measurement values relative to the mean dose-response curve were further investigated to explore the possibility of finding indirect evidence of radiobiologic phenomena related to the detected variance.

For this purpose, a subgroup of patients was formed, where the  $D_{mean}$  for both parotid glands ranged between 10–50 Gy. This was performed to exclude the nearly flat low and high dose regions of the dose-response curve, where there is only a minor change in rEF as the  $D_{mean}$  is changed. Submandibular glands were excluded as only a few patients had  $D_{mean}$  values of both glands less than 50 Gy. Within the dose-restricted subgroup the effect of the mean systematic residual patient positioning error to the  $D_{mean}$  of the glands was evaluated from portal images based on the re-registration by using bony structures in the surroundings of the salivary glands. The  $D_{mean}$  values were then corrected accordingly.

Additionally,  $rEF > 1.3$  values were excluded to remove outliers, as well as the salivary glands which were not functional before the course of RT. The difference  $\Delta rEF$  for each parotid gland  $i$  can be calculated using the equation

$$\Delta rEF_i = rEF_{sc,i} - rEF(D_{mean,i}), \quad (10)$$

where  $rEF_{sc,i}$  is the relative excretion fraction measured by scintigraphy and  $rEF(D_{mean,i})$  represents the value of the mean dose-response function at glandular dose  $D_{mean}$  according to Eq. 8.

Finally, a patient-specific mean  $\Delta rEF$  value ( $\Delta rEF_{mean}$ ) was calculated as an average of all four major salivary glands, including also the submandibular glands. The patients were sorted in ascending order based on the value of  $\Delta rEF_{mean}$ , and three groups of equal size with low, medium and high  $\Delta rEF_{mean}$  were formed in order to evaluate inter-patient variation in  $rEF$ . For each of three groups a new  $D_{50}$  value was determined by re-fitting the sigmoidal dose-response function having both parotid and submandibular glands pooled together and keeping the  $k$  parameter constant.

## 4 Results

### 4.1 Managing organ motion/physiological changes in ART of urinary bladder cancer

#### 4.1.1 Time trends in urinary bladder volume

Changes in the urinary bladder volume and dimensions were determined at different time scales in order to investigate both inter- and intra-fraction patterns of organ motion. Patient data in Studies I and III were pooled together to observe the volumetric changes in the bladder during the course of treatment. Bladder expansion during the time scale of a single treatment fraction was modelled in Study II.

#### Inter-fractional changes

A substantial variation in the volume of an empty bladder was detected (Figure 4-1) with a trend of decreasing bladder volume towards the end of the treatment course. A weekly volume average, calculated as the mean value of bladder volumes for 13 patients during each week of treatment up to the 5<sup>th</sup> treatment week, decreased by 4% per treatment week.

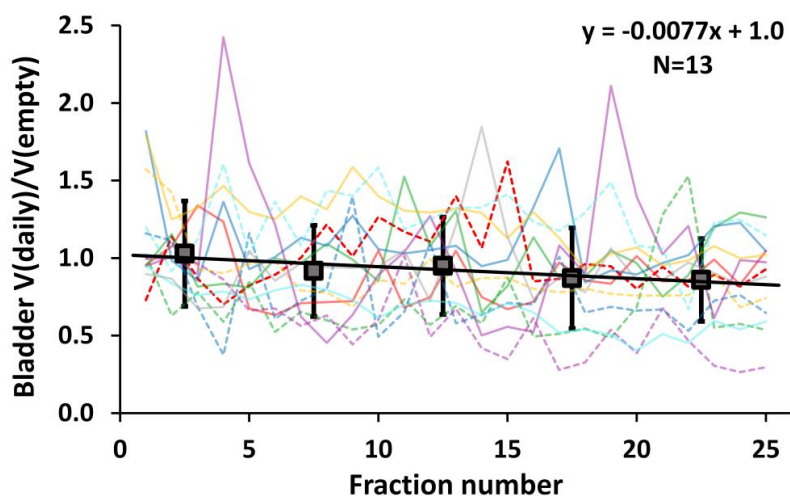


Figure 4-1. The fluctuation of bladder volume during the first 25 fractions (5 weeks of treatment). The colored lines represent the bladder volume determined from the daily CBCT images relative

to the empty bladder volume in the planning CT for 13 individual patients. The black boxes are the weekly averages of all 13 patients, and the error bars represent the standard deviation ( $\pm$ ISD). The regression line represents a linear fit to the daily bladder volumes.

The range of bladder volumes during treatment showed large differences between the patients. The extent of bladder volume variations between treatment fractions was highly correlated ( $R=0.87$ ,  $p=0.0005$ ) with the volume expansion measured during the 45-minute planning CT sequence (Figure 4-2).

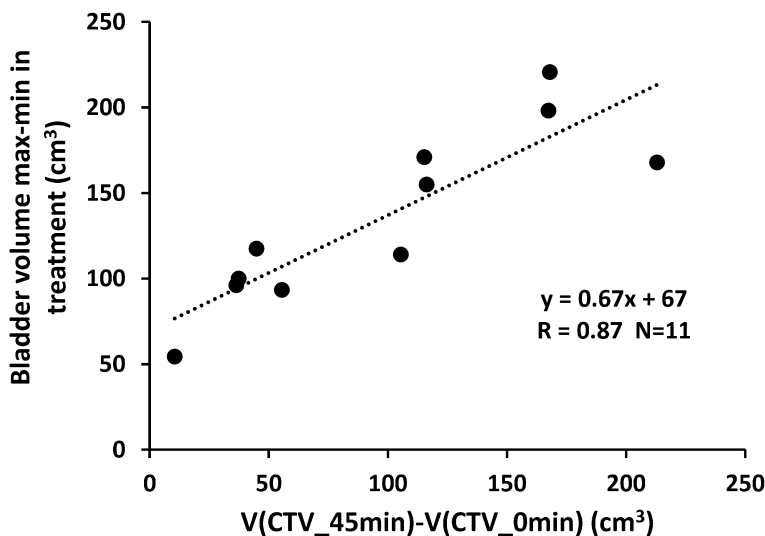


Figure 4-2. The patient-specific ( $N=11$ ) variation of bladder volume (max-min) in daily CBCT images during the course of treatment as a function of bladder volume expansion during the 45-minute treatment planning CT scanning session.

### Intra-fractional changes

The observed enlargement of the bladder diameter between successive CT scans in 15-min intervals varied between the axis of measurement (Table 4-1). The growth was almost symmetric in the AP and LR dimensions. The caudal wall of the bladder did not practically move at all while the cranial part was responsible for the majority of the movement in the CC direction [II]. Considerable variation in the rate of the bladder volume increase was observed with a range of 0.5–4.6 ml/min (mean  $\pm$  SD =  $2.1 \pm 1.3$  ml/min), despite the aimed controlled conditions for hydration. In addition, a large intra-

## RESULTS

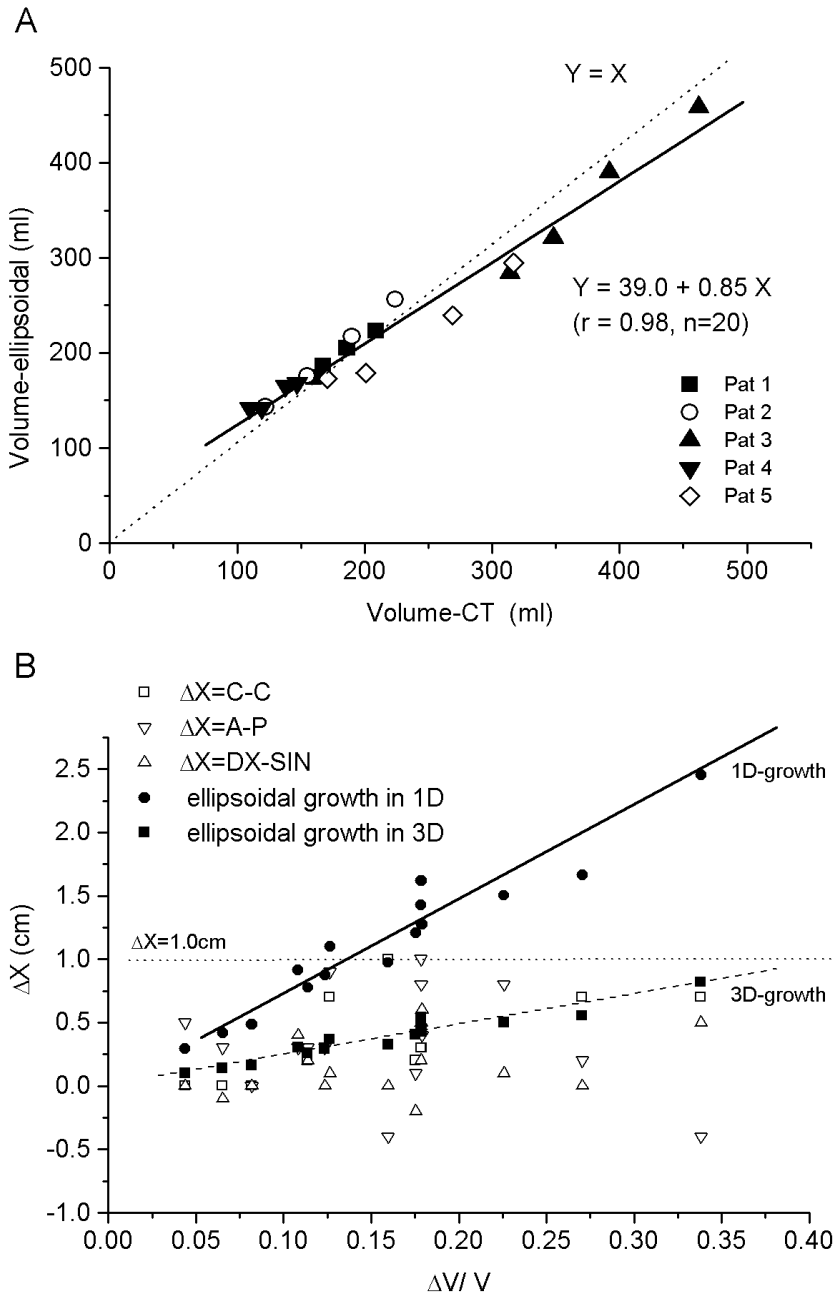
---

patient variation with no clear temporal pattern for the urine formation during the entire 45-min scanning procedure of planning CT was detected [II].

The bladder volume was modelled with an ellipsoidal shape as a function of the true bladder volume determined from the planning CT scans from five patients (Figure 4-3 A). A worst case scenario, where the bladder volume growth was modelled as a mere consequence of growth of one dimension, gave an upper limit for the observed dimensional changes (Figure 4-3 B). The excretion of urine into the bladder during the treatment delivery was mostly slower than during treatment planning CT acquisition (Figure 4-4). On two out of the 25 examined treatment fractions the observed bladder filling clearly exceeded the average filling rate during planning CT. [II].

*Table 4-1. The mean and maximum changes of bladder diameter and standard deviation (SD) during 15-minute intervals between the planning CT acquisitions. Four pairs of successive CT images were analysed for each of the five patients.*

<b>Measurement axis</b>	<b>Mean (mm)</b>	<b>SD (mm)</b>	<b>Max (mm)</b>
<b>cranial-caudal</b>	3.8	2.9	10.0
<b>anterior-posterior</b>	3.4	4.2	9.0
<b>left-right</b>	1.5	2.4	5.0



## RESULTS

Figure 4-3. A) Comparison between the bladder volume modelled as an ellipsoid and actual bladder volume measured in the planning CT scans. B) The changes of the maximum dimensions of the bladder measured in cranial-caudal (C-C), anterior-posterior (A-P) and lateral (DX-SIN) directions (open symbols). All the observed changes lie under the level of 1.0 cm (dotted line). The calculated theoretical limit for the growth in one dimension (one of C-C, A-P or DX-SIN, others unchanged) is plotted in solid circles (fit: solid line) and the theoretical growth in three dimensions (all of C-C, A-P and DX-SIN) is plotted with solid squares (fit: dashed line) (Eqs. (3) and (4)). [11]

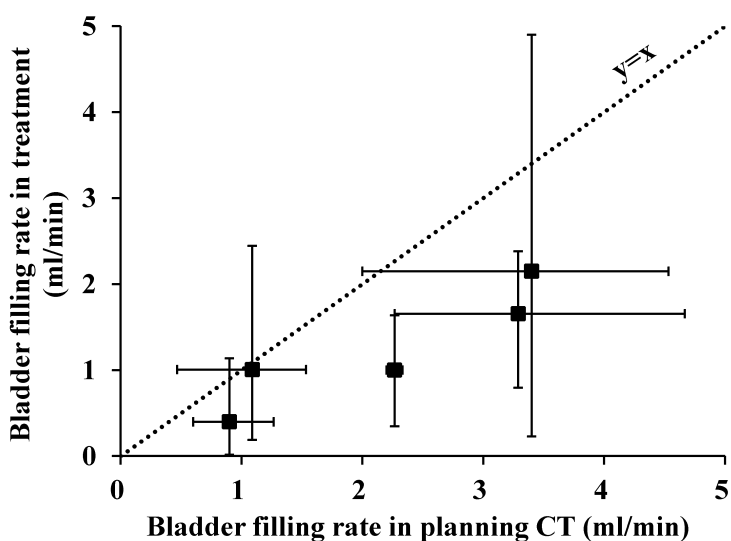


Figure 4-4. The filling rates of the bladder during five treatment fractions of five patients as measured from pre- and post-treatment CBCT images, compared to the bladder volume growth during the 15-minute intervals between the successive planning CT scans. The square symbols mark the mean values and the bars indicate the measured range of the filling rates.

### 4.1.2 The benefits of ART for urinary bladder cancer

#### The volumes of the irradiated normal tissue

The absorbed dose in the IC was considerably lower by using the ART technique as compared to the conventional, non-adaptive technique. A reduction of cumulative dose in IC was observed for all five patients included in the analysis [11] (Figure 4-5 A). On average, the IC volume receiving at least 45 Gy was reduced by 155 cm<sup>3</sup>, with a maximum



reduction of 240 cm<sup>3</sup>. For one patient the PTVs included pelvic lymph nodes, gaining the minimum IC volume sparing of 65 cm<sup>3</sup> at 45 Gy. These values include the effect of partial bladder volume irradiation, since all the boost PTVs were smaller than the conventional PTVs, which were used for the calculation of the comparison DVHs. However, in Figure 4-5 B an additional mean DVH for IC was determined using only the initial part of the treatment excluding the partial bladder boost, similarly showing a large sparing of the IC volume throughout the entire dose range [I].

In Study III, the normal tissue irradiation was also evaluated relative to another plan-library-based ART technique for bladder cancer. The volume of normal tissue inside the high dose region was determined for each treatment fraction as a difference between the daily selected PTV volume and the daily bladder volume as observed in CBCT images (Figure 4-6). For all ten patients included in the analysis, the RepeatCT method (based on a repeated treatment planning CT imaging sequence) produced smaller mean irradiated normal tissue volumes than the RepeatCBCT method (based on one treatment planning CT image combined with repeated CBCT imaging). The volume difference was 80 cm<sup>3</sup> on average ( $p < 0.001$ , paired t-test, two-tailed). Both of the ART methods considerably reduced the volume of normal tissue inside the irradiated high-dose volume as compared to the non-ART method. However, it should be emphasized that in this comparison the CTV-to-PTV margins used for the simulation of the non-ART protocol were larger than the margins previously used at HUCH, resulting in relatively high irradiated volumes for the non-ART method.

### **Dose coverage in urinary bladder**

Dose coverage in bladder was estimated for the first five patients treated using the ART technique [I]. The near-minimum dose as described in ICRU 83 report [71] was used in this thesis for the evaluation of dose coverage. Defining a geographical miss as 98% of the urinary bladder volume receiving less than 95% of the prescribed dose, no statistically significant difference was observed in the rate of geographical miss between the adaptive and non-adaptive treatments (3 and 4 fractions out of 125, respectively,  $p = 1.000$ , McNemar test).

RESULTS

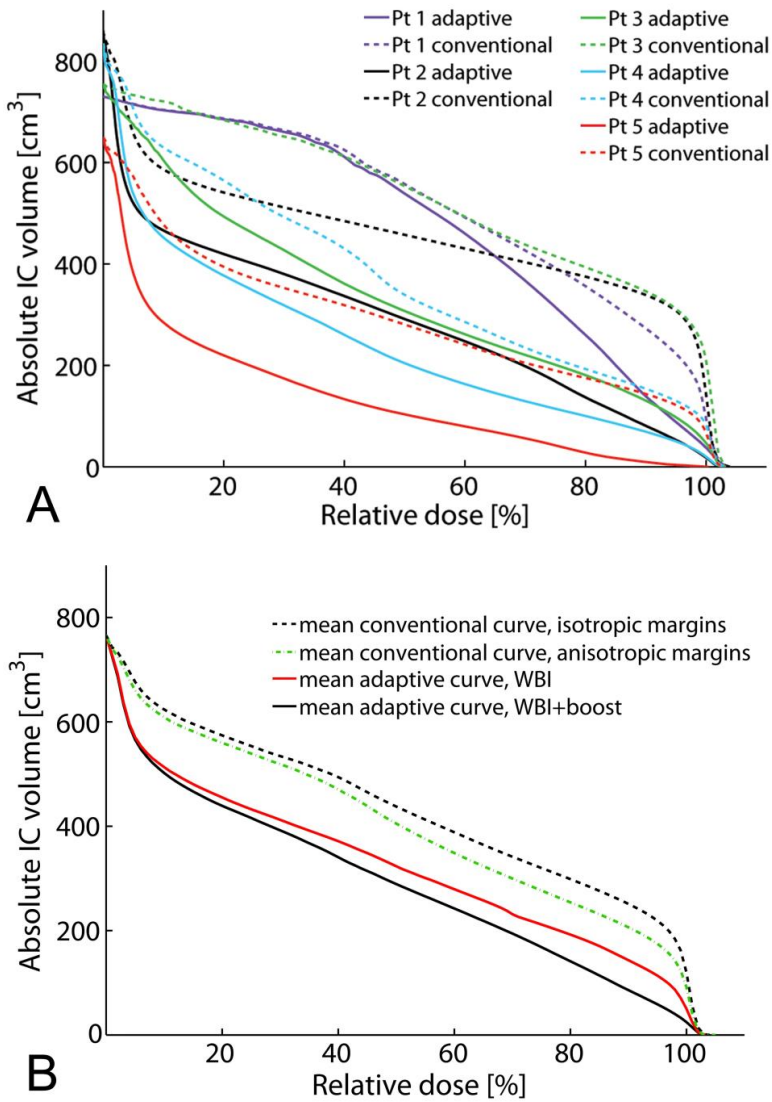


Figure 4-5. Cumulative DVHs for the intestinal cavity (IC) volume, where the dose is presented as a percentage of the total prescription dose. A) Two curves are presented for each patient: the ‘adaptive’ curves are calculated using the daily adaptive treatment plans, and for comparison the ‘conventional’ curves are calculated using a single non-adaptive treatment plan with isotropic 20 mm PTV margins. B) The mean cumulative DVHs of IC volumes are calculated as an average of all five patients. Two different CTV-to-PTV margins (isotropic and anisotropic)

are used to form the non-adaptive mean curves (dotted lines). Two adaptive curves are also determined (solid lines): one including only the elective part of the treatment (WBI, whole bladder irradiation) and one for the entire treatment including the whole bladder irradiation and the partial bladder boost (WBI+boost). [1]

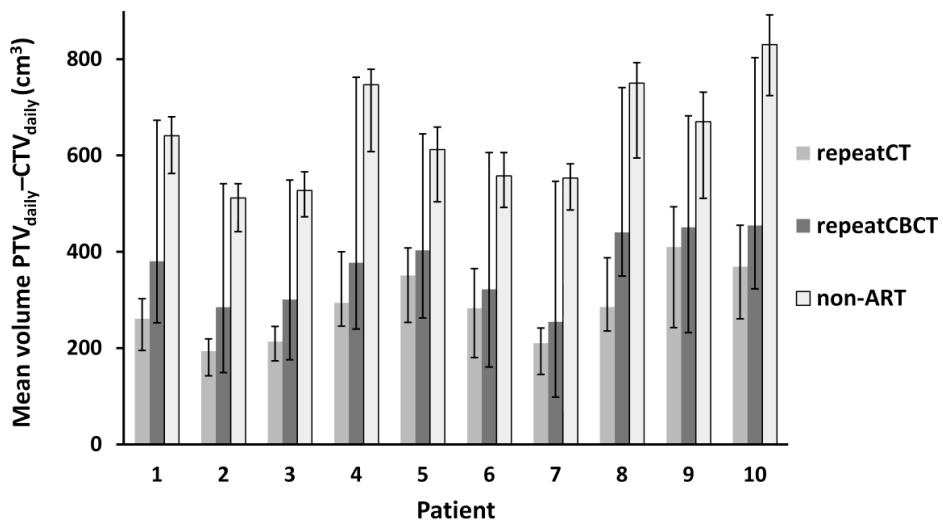


Figure 4-6. The mean volumes  $PTV_{daily} - CTV_{daily}$  ( $cm^3$ ), averaged across all 30 treatment fractions, for the two compared ART methods (repeatCT and repeatCBCT) and a non-ART method. These volumes represent the mean volume of normal tissue inside PTV. The error bars indicate the volume range. The figure is modified from Study III.

## 4.2 Predicting salivary gland function in risk-adapted RT of head and neck cancers

### 4.2.1 Individual salivary flow model

The post-RT rates of the absolute excreted saliva volume under stimulation were calculated using Eq. (9) with the sigmoidal dose-response function parameters reported in [68]. The predicted and measured values are presented in Figure 4-7 for 46 patients with a complete set of scintigraphy and salivary flow measurements at the time points of 6 and 12 months after RT. A significant linear correlation was found between the modelled and the directly measured salivary flow rates both six and twelve months after RT. The mean prediction errors for the model were 0.45 and 0.36 ml/min for the predicted salivary flow 6 and 12 months after RT, respectively.

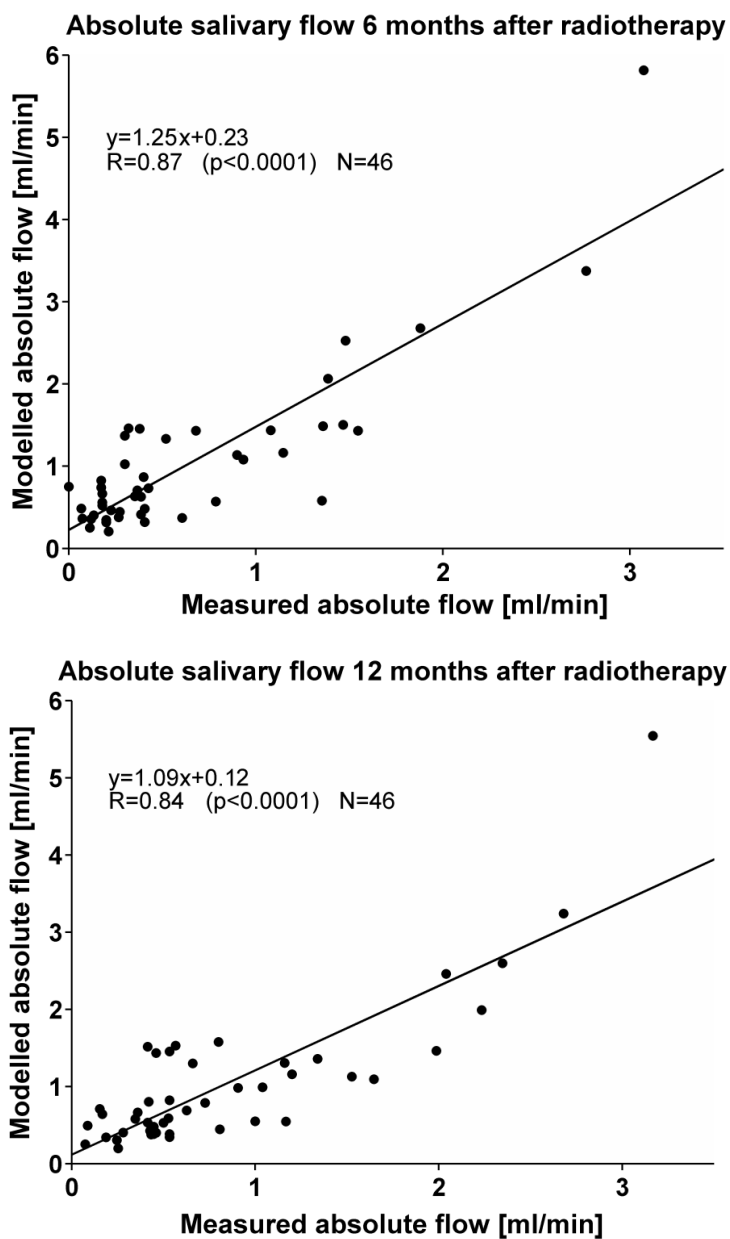


Figure 4-7. A significant linear correlation was seen between the modelled absolute salivary flow ( $F_{calc}$ ) and the measured values of salivary flow ( $F_{meas}$ ) both 6 and 12 months after RT.

#### 4.2.2 Patient-specific variation in salivary gland scintigraphy

To further investigate the differences in patients' post-RT salivary function,  $\Delta rEF$  values, defined as the difference between the  $rEF$  value measured by scintigraphy and the corresponding population mean  $rEF$  value at the same glandular dose, were defined for the parotid glands. In the pairwise comparison of the left and right parotid glands, the  $\Delta rEF$  values were linearly correlated both 6 and 12 months after RT ( $R=0.53$ ,  $p=0.0006$  and  $R=0.79$ ,  $p<0.0001$ , respectively). Additionally, the  $\Delta rEF$  values were compared for the same parotid gland at two different times of measurement (6 and 12 months after RT), showing a linear correlation ( $R=0.53$ ,  $p<0.0001$ ). In Figure 4-8, the  $sEF$  values measured by scintigraphy are presented for the major salivary glands 6 and 12 months after RT. The repeatability of the scintigraphic excretion fraction measurement is moderate, as a good positive correlation was shown between the two measurements at different times. Minor recovery of the salivary gland function was detected between the period of 6 and 12 months after RT (from 0.22 to 0.25 on average,  $p=0.0008$ , two-tailed paired t-test).

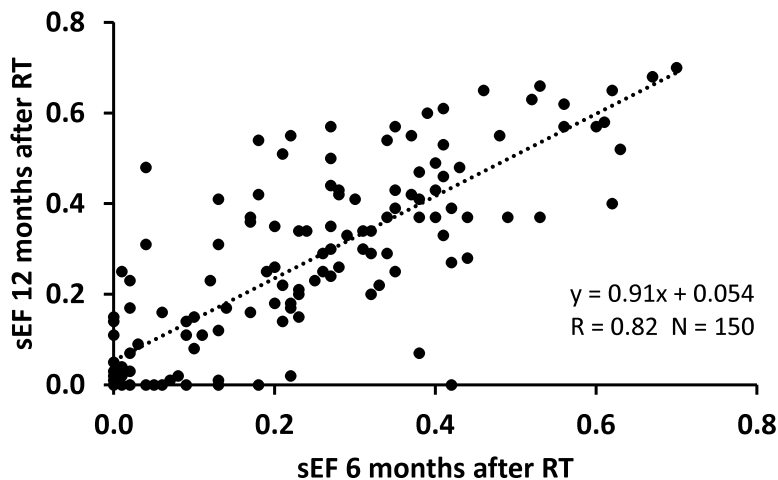


Figure 4-8. A positive linear correlation ( $R=0.82$ ,  $p<0.0001$ ) was established between the scintigraphy  $sEF$  measurements at 6 and 12 months after RT, reflecting a moderate stability of the measurement technique. Mean  $sEF$  values were 0.22 and 0.25 at 6 and 12 months after RT, respectively, showing a mild recovery of the salivary gland function ( $p=0.0008$ , pairwise t-test, two-tailed).

## RESULTS

For some patients the measured post-RT rEF values of the both parotid glands (left and right) were clearly either above or below the mean dose-response curve. This behaviour was present at both times of measurement (6 and 12 months after RT). Hence, it was concluded that the systematic differences found in  $\Delta rEF$  values between the patients were not generated by transient instabilities in the scintigraphy measurement technique. From these results it was deduced that there can be some biological factor, such as intrinsic radiosensitivity, that affects the post-RT scintigraphy results.

In further evaluation of inter-patient differences in post-RT salivary gland function,  $\Delta rEF_{\text{mean}}$  calculated as an average of all the functioning major salivary glands was used. The patients were divided into three groups of equal size with low, medium and high  $\Delta rEF_{\text{mean}}$ , with an average  $\Delta rEF_{\text{mean}}$  value of -0.25, 0.02 and 0.24, respectively. The re-fitting of a sigmoidal dose-response function resulted in  $D_{50}$  values of 23, 36 and 42 Gy for the low, medium and high  $\Delta rEF_{\text{mean}}$  groups, respectively (Figure 4-9). These values correspond to the absorbed doses causing a fifty-percent degradation of sEF in the three groups. This gives an idea of the range of variation in an individual patient's response to RT.

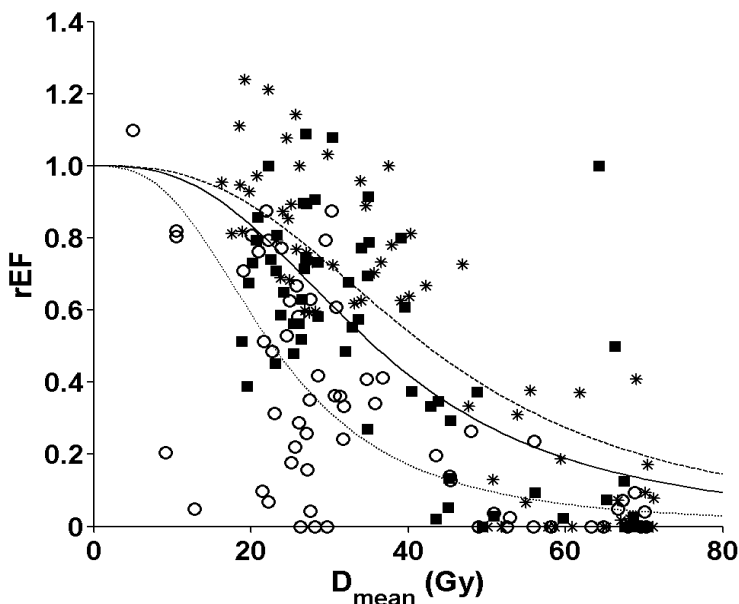


Figure 4-9. Relative excretion fraction (rEF) for individual salivary glands with the patients divided into three groups: low  $\Delta rEF_{\text{mean}}$  (open circles), medium  $\Delta rEF_{\text{mean}}$  (filled squares) and high  $\Delta rEF_{\text{mean}}$  (asterisks). A sigmoidal dose-response function is plotted for the three separate groups yielding  $D_{50}$  values of 23, 36 and 42 Gy for the respective groups.

## 5 Discussion

In the following the results presented in this thesis are discussed and critically evaluated, taking the limitations of the performed measurements and analysis into account. In addition, aspects for future development and possible applications are discussed.

### *5.1 Changes of bladder dimensions between and during RT treatment fractions*

Even though the patients were instructed to empty their bladder before each treatment fraction, considerable variation in the bladder volume was present during the course of RT. The difficulty of maintaining constant bladder volume throughout RT has been widely recognised in the literature over time [72-76]. One appealing solution in the attempt of standardizing the bladder volume for the entire course of RT would be catheterization. However, the use of indwelling catheters has been associated with infections of the urinary tract [77]. In this study, some patients showed clearly more fluctuation in the bladder volume than the others. Also, the measured bladder volume expansion during the acquisition of four planning CTs correlated with the range of bladder volumes during treatment. In future, this information could be used to limit the number of treatment plans in the library for those patients whose bladder showed only modest expansion between planning CTs.

As RT is usually the choice of treatment for patients unfit for cystectomy, in this population the patients often have several co-morbidities that may influence the patient's ability to void. For example, one patient showing the largest variation in bladder size was disabled, and voiding the bladder exactly at the right moment may have been difficult. Some of the detected large volumes were also related to the intensive hydration during chemotherapy. Nevertheless, the fact that for most of the patients the bladder volumes could not be controlled by merely giving instructions about voiding, demonstrates the need for an adaptive strategy for this particular tumour site.

The intra-fractional expansion of the bladder was investigated in this research by observing the changes in the bladder dimensions between successive planning CTs. This yielded further information about the dimensional changes related to different bladder volumes from an empty to a full bladder. In addition, it was verified that the bladder filling rate was generally lower in the treatment than during planning CT acquisition. The

## DISCUSSION

---

values in Table 4-1 give the measured maximal changes of the bladder diameter during the 15-minute intervals. In the sample of five patients, the dimensional changes in LR and AP directions were found to be mostly symmetric. Hence, using a soft tissue matching protocol in the treatment, the 10 mm maximum expansion can be divided in half (5 mm) to give the intra-fractional margin in the LR and AP directions. In the treatment setup applied at HUCH, a 10 mm margin should be added in the cranial direction to account for intra-fractional filling and bladder deformation, and in the caudal direction the margin can be less than 3 mm. These margins would cover all of the detected intra-fractional changes in the treatment set-up applied at HUCH, and they are only adequate for the maximum time of 15 minutes elapsed from the acquisition of CBCT to the end of irradiation. However, as the number of patients included in the study is very small, any general recommendations about the intra-fractional margins applied for bladder ART cannot be given. Instead, the aim was to verify that the CTV-to-PTV margins used in the bladder ART protocol at HUCH were adequate. According to this study the margins used were generous and they could even be reduced in the lateral and posterior directions. Other studies have addressed intra-fractional expansion of the bladder using MR [73,78,79] or CT imaging [76,80]. Intra-fractional margins of 5-6 mm have been suggested in the literature [79,80]. Nevertheless, the magnitude of these margins depends on the conformity of the applied treatment technique (3D conformal, IMRT or VMAT).

### *5.2 ART workflow for urinary bladder cancer implemented at HUCH*

The first bladder cancer patients were treated at HUCH in 2009 using the described ART protocol. Thus, the HUCH Cancer Center was among the first clinics in the world to implement a plan-library-based ART for urinary bladder cancer. The applied workflow has evolved during the years, including the planning CT procedure, the choice of treatment technique, the online matching procedure and the plan selection criteria. At first, several planning CT intervals were tested, starting from a 30-minute interval between the successive scans. However, quite soon this was gradually reduced to 15 minutes, which was found to be optimal both in terms of the patients' ability to hold the urine during bladder filling and both personnel and time resources of the department. At the same time, the amount of water intake right before the first CT scan was increased from 2 dl to 8 dl. The treatment technique was changed from IMRT to VMAT in 2011, enabling faster treatment delivery. At very early stage of implemented ART, the matching of daily CBCT to planning CT image was performed using bony structures. Nevertheless, rather soon it became obvious that occasionally some manual adjustments were required during the matching procedure due to variable rectum filling leading to bladder shifting or deformation. Finally, it was decided to apply full soft tissue matching to compensate



for changes in rectum filling. For the first five patients treated with ART, the criterion for the plan selection was different than for the subsequent patients. For these patients, the smallest PTV encompassing the entire bladder with at least a 3-mm margin was selected. This intra-fractional margin of 3 mm was derived from the literature as an average movement of the bladder wall between pre- and post-RT CBCT [81]. However, the adequacy of this intra-fractional margin was later questioned, and full CTV-to-PTV margins were exploited by selecting the plan using the CTV contour which was the closest match to the daily bladder volume.

According to this study, regardless of the CTV-to-PTV margin reduction from 20 mm isotropic to 10–15 mm anisotropic margin, the dose coverage of the urinary bladder was not compromised when changing from the non-adaptive treatment technique to ART. The absorbed dose to the IC was evaluated by direct summation of single fraction DVHs based on daily contours of bowel cavity. This procedure yields a rough approximation of the cumulative dose in a worst case scenario where the highest dose always affects the same part of the bowel cavity. Nowadays, there are deformable registration algorithms available in commercial software, enabling cumulative dose tracking for individual voxels of interest [82]. However, due to the constant peristaltic motion and deformation of the small bowel, tracking the dose for the intestines would be challenging at least, if not impossible. Several studies have addressed the topic of normal tissue sparing in bladder ART [24,35,38,40,83]. Yet, only a few studies have based their evaluation on daily DVH curves for the OARs as seen in the CBCTs [40,83], and Study I was the first to report clinical results using this approach. In the presented research a large reduction in the irradiated IC volume was seen, which was similar to the results obtained in other studies [38,40].

A clinically interesting comparison was made between the ART protocol applied at HUCH (RepeatCT) and another plan-library-based protocol that had been used at AUH (RepeatCBCT) [84]. The aim of this study was to determine whether one of the methods of creating the adaptive PTVs was superior in terms of normal tissue sparing and range of different PTV volumes. To manage this simulation study, some alterations in the original workflows had to be done, and hence the clinically used methods could not be compared directly. A significant difference was found in the volume of the irradiated normal tissue, in favour of the RepeatCT method. However, for some patients the repeated planning CT sequence failed to predict the bladder shape during the course of treatment, causing even the largest PTV to be inadequate to cover the entire bladder for a few fractions. For these few patients the RepeatCBCT method yielded a more suitable selection of different PTV shapes. If the shape of the bladder is radically different from

## DISCUSSION

---

the planning CTs during the first treatment fractions, it could be recommended that two additional adaptive PTVs should be added in the RepeatCT library using the RepeatCBCT method for PTV definition. At HUCH the RepeatCT method has been found to be more appealing, as it leaves more time for performing the contouring and treatment planning, and provides better image quality for contouring. In addition, as some of the elderly patients receive moderately hypofractionated RT, a protocol starting the ART right from the first treatment fraction can be beneficial.

As a non-standard method, plan-library-based ART requires special attention at all stages of the RT to avoid errors. At the moment, all commercial treatment verification systems do not adequately support the use of several alternative treatment plans. Therefore, additional care is required from the therapists to pick and deliver the correct treatment plan from the verification system. The patients included in this research have been treated partly by using the Varian Clinac iX linac connected to ARIA verification system, and partly by using the Elekta Axesse linac together with the Mosaiq verification system. It is essential, that in the near future the commercial software manufacturers would find a better way to support the use of treatment plan libraries.

Plan-library-based ART may be seen as a transition phase towards daily online re-optimization of the treatment plans based on pre-fraction imaging. However, implementation of such online ART strategies requires a lot of effort before they will be ready to be introduced to clinical routine. Even if all the technical challenges, such as rapid and reliable deformable registration, fast online re-optimization, dose accumulation and quality assurance (QA) could be resolved, the question of who takes responsibility for the daily contours and the treatment plans still remains. A plan-library-based approach for the ART of urinary bladder cancer is a robust method that requires relatively small effort for its implementation. An additional advance of this method is that QA for the treatment plans can be performed before the initiation of the treatment course. Therefore, this approach can be expected to remain as the state-of-the-art method also in the future. The method is applicable for other tumour sites as well [26,85,86], and the future plan at HUCH is to implement a similar approach to cervical cancer.

### *5.3 Prediction of salivary flow after RT of head and neck region*

A step towards risk-adaptive RT for head and neck cancers was taken by constructing a predictive model for post-RT saliva excretion. A significant correlation was established between the predicted and measured values of salivary flow. The idea behind this model was to determine the contribution of each individual salivary gland to the total saliva

output by a pre-RT scintigraphy measurement. These proportional values were then scaled using the estimated population-based dose-response functions. This approach differs from many other published salivary function models [87-91]. In the generally used normal tissue complication probability models, a single endpoint is selected to represent the radiation-induced complication [60,92]. For example, in a model for salivary function, a 75% loss of saliva excretion could be considered as a complication. The advantage of our model is that it describes salivary function in a continuous manner, and no threshold value needs to be introduced to define the presence of a complication.

However, the predicted values of saliva excretion did not have a perfect correspondence with the measured ones. Therefore, also the patient-specific variation in the scintigraphy measurements was investigated. For this purpose, the distances of the rEF values for the individual glands from the mean dose-response curves were determined in order to see if all four major salivary glands of an individual patient behave similarly. In this analysis, a common pattern of reaction of individual glands was detected. Hence, there may be a common factor, such as a patient-specific sensitivity, which may explain the similar deviation of separate glands from the mean dose-response curve when compared to each other at the same time point, and even at two different time points. It is unlikely that some other unknown random factor, such as the consistence of the stimulus, the daily variation of the patient's response to the stimulus or any variation related to the scintigraphic analysis, would cause a similar effect in both bilateral glands at two different times of measurement. Hence, this result can be considered as indirect evidence for some mechanism of patient-specific sensitivity that each gland follows.

Three different patient groups were artificially formed based on the use of  $\Delta rEF_{\text{mean}}$  value calculated for all four major salivary glands. These groups consisted of patients having high, medium and low dose-response as compared to the population average. The purpose of this analysis was to give an idea of the variation in data and  $D_{50}$  doses due to possible patient-specific sensitivity to radiation. The  $D_{50}$  values given by the analysis were 23, 36 and 42 Gy for the different groups, respectively. However, these data include the overall uncertainty of the method, and the contribution of radiosensitivity could not be exclusively extracted. As an additional experiment, absolute salivary flow was recalculated using the separate  $D_{50}$  values for the three patient groups. This resulted in a clearly better agreement between the calculated and measured values for the groups with low and high dose-response. This supports the idea that if we had a-priori knowledge about individual radiosensitivity of the patients, and it could be quantified and taken into account in the predictive model, the accuracy of the model could possibly be improved.

## DISCUSSION

---

The limitations of the performed analysis include the large uncertainty of the scintigraphic measurements. In a study by Firat *et al.* [93], applying a similar technique to ours, a SD of 0.09-0.14 in sEF was observed in different age groups of normal subjects for both parotid and submandibular glands. A SD of 0.14 in sEF corresponds to a SD of 0.2 for rEF, which is calculated as a ratio of two sEFs. The true SD is likely to be smaller for the relative values, as the variance in sEF also includes possible inter-patient variations in the reaction to the stimuli, which is eliminated in rEF. Hence, 0.2 can be estimated to give an absolute upper limit for the variation in rEF. In our scintigraphy data, the standard error for the fit of the sigmoidal dose-response curve was 0.42 for the parotid glands. This suggests that there remains a large component of variation, which cannot be explained by the measurement technique, and this could be partly due to radiosensitivity. The effect of smoking to the dose-response was not investigated in this study.

In the pairwise analysis of parotid glands, the effect of mean systematic residual patient positioning error to the  $D_{mean}$  of the glands was evaluated from portal images using the bony structures close to the parotid glands for matching, and the  $D_{mean}$  values were corrected accordingly. In dose accumulation studies, even quite large discrepancies between the planned and actually delivered  $D_{mean}$  doses have been reported. However, when the calculated doses are compared to the delivered ones rather complex positional changes, such as rotations of the neck or head, may have a large impact on the dose delivered to the glands, if the patient positioning has been done according to the cervical vertebrae. In a dose accumulation study by Hunter *et al.* [70], the median delivered mean parotid dose increased by 0.9 Gy, which is in accordance with other similar studies. The complex setup deviations were identified as a major cause for the large dose discrepancies, as the large dose differences were already present in the first treatment fraction. In our analysis, the mean effect of the setup deviations in parotid  $D_{mean}$  was estimated. Hence, possible errors in the  $D_{mean}$  values in the present analysis are mainly due to the possible shrinkage and shifting of the glands. In the literature, this has been given a mean value of 3 mm towards the midline, which in our patient data corresponds to a dose increase of 1.2 Gy [69,94]. As the slope of the dose-response curve for parotid glands was not very steep, an error of this magnitude in  $D_{mean}$  would not have a large effect in  $\Delta rEF$ . Also, as shrinkage and shifting of the parotid glands would increase the  $D_{mean}$ , it cannot explain the large positive  $\Delta rEF$  values. Interestingly, in the study by Hunter *et al.* [70], the use of the actual delivered doses did not decrease the large dispersion of the dose-effect data points in salivary output measurements. This may be true for scintigraphic measurements as well, and it provides support for the idea of radiosensitivity being one of the factors explaining the variation in post-RT saliva secretion.

Encouraged by this research, systematic pre-RT salivary gland scintigraphy was recently initiated for all head and neck cancer patients at HUCH. The aim is to find out which salivary glands have the largest effect on the total saliva output. Then, if possible, the treatment plan could be adjusted so that the post-RT saliva excretion can be maximized without compromising the target dosage.

At HUCH, there is an ongoing research project, where the pre-RT salivary gland function has been measured both using scintigraphy and diffusion-weighted MRI. It would be optimal to find a quantitative indicator of salivary function on MRI, which could be used for modelling of the post-RT salivary function. Thus, the salivary gland scintigraphy could be replaced with a non-irradiative procedure. The MRI also provides volumetric image with high spatial resolution, enabling separation of different functional volumes inside the salivary gland. A plan for the near future is to investigate the possible regional differences within the glands and how they could affect the dose-response of the salivary glands, with the aim of increasing the potential for risk-adapted RT in the head and neck region.

### 6 Conclusions

In the present thesis, two methods for incorporating individual physiological changes in RT treatment planning were developed. Both suggested methods aimed at reducing dose to the normal tissues. The first method, ART for urinary bladder cancer, was implemented and found feasible for routine clinical use. The second method was designed to aid treatment planning for head and neck cancers. The thesis reached its aims with the following main conclusions:

- 1) The inter- and intra-fractional changes in the urinary bladder were quantified in order to take them into account in ART for urinary bladder cancer. Considerable variation was detected in the volumes of residual urine in the voided bladders, which pointed out the need for an adaptive treatment strategy. An investigation of the intra-fractional variations in the urinary bladders confirmed the adequacy of the applied CTV-to-PTV margin,
- 2) A plan-library-based workflow of ART for urinary bladder cancer was clinically implemented at HUCH. It was shown to reduce the absorbed dose to the IC, while the dose coverage in the bladder remained at the same level as in the conventional, non-adaptive method. The method applied at HUCH was compared with another clinically implemented plan-library-based method, resulting in a significant difference in the volumes of irradiated normal tissue, in favour of the HUCH method, and
- 3) A clinically feasible method of predicting post-RT saliva excretion was developed by using the pre-RT measurements of salivary gland function and the dose information from treatment plans. A good correlation between the modelled and measured values of salivary flow was established. A partly unexplained variation was present in the post-RT excretion fraction values measured with scintigraphy. This was considered as indirect evidence of the possibility of patients' intrinsic individual radiosensitivity having an effect on post-RT salivary function.

---

## References

- [1] Khan FM. The physics of radiation therapy. Philadelphia, US: Lippincott Williams and Wilkins. 2010.
- [2] Bel A, Van Herk M, Lebesque JV. Target margins for random geometrical treatment uncertainties in conformal radiotherapy. *Med Phys* 1996;23:1537-1545.
- [3] Stroom JC, de Boer HCJ, Huizenga H, Visser AG. Inclusion of geometrical uncertainties in radiotherapy treatment planning by means of coverage probability. *Int J Radiat Oncol Biol Phys* 1999;43:905-919.
- [4] van Herk M, Remeijer P, Rasch C, Lebesque JV. The probability of correct target dosage: dose-population histograms for deriving treatment margins in radiotherapy. *Int J Radiat Oncol Biol Phys* 2000;47:1121-1135.
- [5] van Herk M. Errors and margins in radiotherapy. *Semin Radiat Oncol* 2004;14:52-64.
- [6] Stroom J, Gilhuijs K, Vieira S et al. Combined recipe for clinical target volume and planning target volume margins. *Int J Radiat Oncol Biol Phys* 2014;88:708-714.
- [7] Yan D, Vicini F, Wong J, Martinez A. Adaptive radiation therapy. *Phys Med Biol* 1997;42:123-132.
- [8] Thörnqvist S, Hysing LB, Tuomikoski L et al. Adaptive radiotherapy strategies for pelvic tumors – a systematic review of clinical implementations. *Acta Oncol* 2016;55:943-58.
- [9] Langen KM, Jones DTL. Organ motion and its management. *Int J Radiat Oncol Biol Phys* 2001;50:265-278.
- [10] van Herk M, Bruce A, Guus Kroes AP, Shouman T, Touw A, Lebesque JV. Quantification of organ motion during conformal radiotherapy of the prostate by three dimensional image registration. *Int J Radiat Oncol Biol Phys* 1995;33:1311-1320.
- [11] Roeske JC, Forman JD, Mesina CF et al. Evaluation of changes in the size and location of the prostate, seminal vesicles, bladder, and rectum during a course of external beam radiation therapy. *Int J Radiat Oncol Biol Phys* 1995;33:1321-1329.
- [12] Pos FJ, Koedooder K, Hulshof MCCM, van Tienhoven G, González González D. Influence of bladder and rectal volume on spatial variability of a bladder tumor during radical radiotherapy. *Int J Radiat Oncol Biol Phys* 2003;55:835-841.

## REFERENCES

---

- [13] Fokdal L, Honoré H, Høyer M, Meldgaard P, Fode K, von der Maase H. Impact of changes in bladder and rectal filling volume on organ motion and dose distribution of the bladder in radiotherapy for urinary bladder cancer. *Int J Radiat Oncol Biol Phys* 2004;59:436-444.
- [14] Gwynne S, Webster R, Adams R, Mukherjee S, Coles B, Staffurth J. Image-guided radiotherapy for rectal cancer — A Systematic review. *Clin Oncol* 2012;24:250-260.
- [15] Jadon R, Pembroke CA, Hanna CL et al. A systematic review of organ motion and image-guided strategies in external beam radiotherapy for cervical cancer. *Clin Oncol* 2014;26:185-196.
- [16] Yan D, Ziaja E, Jaffray D et al. The use of adaptive radiation therapy to reduce setup error: a prospective clinical study. *Int J Radiat Oncol Biol Phys* 1998;41:715-720.
- [17] Pötter R, Knocke TH, Fellner C, Baldass M, Reinthaller A, Kucera H. Definitive radiotherapy based on HDR brachytherapy with iridium 192 in uterine cervix carcinoma: report on the Vienna University Hospital findings (1993–1997) compared to the preceding period in the context of ICRU 38 recommendations. *Cancer/Radiothérapie* 2000;4:159-172.
- [18] Pos FJ, Hulshof M, Lebesque J et al. Adaptive radiotherapy for invasive bladder cancer: A feasibility study. *Int J Radiat Oncol Biol Phys* 2006;64:862-868.
- [19] Nijkamp J, Pos FJ, Nuver TT et al. Adaptive radiotherapy for prostate cancer using kilovoltage cone-beam computed tomography: first clinical results. *Int J Radiat Oncol Biol Phys* 2008;70:75-82.
- [20] Foroudi F, Wong J, Haworth A et al. Offline adaptive radiotherapy for bladder cancer using cone beam computed tomography. *J Med Imaging Radiat Oncol* 2009;53:226-233.
- [21] Schwartz DL, Garden AS, Shah SJ et al. Adaptive radiotherapy for head and neck cancer—Dosimetric results from a prospective clinical trial. *Radiother Oncol* 2013;106:80-84.
- [22] Tvillum M, Khalil AA, Møller DS, Hoffmann L, Knap MM. Clinical outcome of image-guided adaptive radiotherapy in the treatment of lung cancer patients. *Acta Oncol* 2015;54:1430-1437.
- [23] Nyeng TB, Nordmark M, Hoffmann L. Dosimetric evaluation of anatomical changes during treatment to identify criteria for adaptive radiotherapy in oesophageal cancer patients. *Acta Oncol* 2015;54:1467-1473.



- [24] Foroudi F, Wong J, Kron T et al. Online adaptive radiotherapy for muscle-invasive bladder cancer: Results of a pilot study. *Int J Radiat Oncol Biol Phys* 2011;81:765-771.
- [25] Meijer GJ, van der Toorn P, Bal M, Schuring D, Weterings J, de Wildt M. High precision bladder cancer irradiation by integrating a library planning procedure of 6 prospectively generated SIB IMRT plans with image guidance using lipiodol markers. *Radiother Oncol* 2012;105:174-179.
- [26] Heijkoop ST, Langerak TR, Quint S et al. Clinical implementation of an online adaptive plan-of-the-day protocol for nonrigid motion management in locally advanced cervical cancer IMRT. *Int J Radiat Oncol Biol Phys* 2014;90:673-679.
- [27] Acharya S, Fischer-Valuck BW, Kashani R et al. Online magnetic resonance image guided adaptive radiation therapy: First clinical applications. *Int J Radiat Oncol Biol Phys* 2016;94:394-403.
- [28] Finnish Cancer Registry. Cancer Statistics. 05.03.2016. Available from: URL: <http://www.cancer.fi/syoparekisteri/en/statistics>
- [29] Halperin EC, Brady LW, Perez CA, Wazer DE. *Perez and Brady's principles and practice of radiation oncology*. Philadelphia: Wolters Kluwer/Lippincott Williams & Wilkins. 2013.
- [30] Kaufman DS, Shipley WU, Feldman AS. Bladder cancer. *Lancet* 2009;374:239-249.
- [31] James ND, Hussain SA, Hall E et al. Radiotherapy with or without chemotherapy in muscle-invasive bladder cancer. *N Engl J Med* 2012;366:1477-1488.
- [32] Smith ZL, Christodouleas JP, Keefe SM, Malkowicz SB, Guzzo TJ. Bladder preservation in the treatment of muscle-invasive bladder cancer (MIBC): a review of the literature and a practical approach to therapy. *BJU Int* 2013;112:13-25.
- [33] Meijer GJ, Rasch C, Remeijer P, Lebesque JV. Three-dimensional analysis of delineation errors, setup errors, and organ motion during radiotherapy of bladder cancer. *Int J Radiat Oncol Biol Phys* 2003;55:1277-1287.
- [34] Muren LP, Smaaland R, Dahl O. Organ motion, set-up variation and treatment margins in radical radiotherapy of urinary bladder cancer. *Radiother Oncol* 2003;69:291-304.
- [35] Burrige N, Amer A, Marchant T et al. Online adaptive radiotherapy of the bladder: Small bowel irradiated-volume reduction. *Int J Radiat Oncol Biol Phys* 2006;66:892-897.

## REFERENCES

---

- [36] Redpath AT, Muren LP. CT-guided intensity-modulated radiotherapy for bladder cancer: Isocentre shifts, margins and their impact on target dose. *Radiother Oncol* 2006;81:276-283.
- [37] Sur RK, Clinkard J, Jones WG et al. Changes in target volume during radiotherapy treatment of invasive bladder carcinoma. *Clin Oncol* 1993;5:30-33.
- [38] McDonald F, Lalondrelle S, Taylor H et al. Clinical implementation of adaptive hypofractionated bladder radiotherapy for improvement in normal tissue irradiation. *Clin Oncol* 2013;25:549-556.
- [39] Hafeez S, Warren-Oseni K, McNair HA et al. Prospective study delivering simultaneous integrated high-dose tumor boost ( $\leq 70$  Gy) with image guided adaptive radiation therapy for radical treatment of localized muscle-invasive bladder cancer. *Int J Radiat Oncol Biol Phys* 2016;94:1022-1030.
- [40] Vestergaard A, Muren LP, Lindberg H et al. Normal tissue sparing in a phase II trial on daily adaptive plan selection in radiotherapy for urinary bladder cancer. *Acta Oncol* 2014;53:997-1004.
- [41] Murthy V, Master Z, Adurkar P et al. 'Plan of the day' adaptive radiotherapy for bladder cancer using helical tomotherapy. *Radiother Oncol* 2011;99:55-60.
- [42] Vestergaard A, Muren LP, Søndergaard J, Elstrøm UV, Høyer M, Petersen JB. Adaptive plan selection vs. re-optimisation in radiotherapy for bladder cancer: A dose accumulation comparison. *Radiother Oncol* 2013;109:457-462.
- [43] Vestergaard A, Hafeez S, Muren LP et al. The potential of MRI-guided online adaptive re-optimisation in radiotherapy of urinary bladder cancer. *Radiother Oncol* 2015;118:154-159.
- [44] Søvik Å, Malinen E, Rune Olsen D. Adapting biological feedback in radiotherapy. *Semin Radiat Oncol* 2010;20:138-146.
- [45] Partridge M, Yamamoto T, Grau C, Høyer M, Muren LP. Imaging of normal lung, liver and parotid gland function for radiotherapy. *Acta Oncol* 2010;49:997-1011.
- [46] Eschmann SM, Paulsen F, Bedeshem C et al. Hypoxia-imaging with  $^{18}\text{F}$ -Misonidazole and PET: Changes of kinetics during radiotherapy of head-and-neck cancer. *Radiother Oncol* 2007;83:406-410.
- [47] Harry VN, Semple SI, Gilbert FJ, Parkin DE. Diffusion-weighted magnetic resonance imaging in the early detection of response to chemoradiation in cervical cancer. *Gynecol Oncol* 2008;111:213-220.

- [48] Kim S, Loevner L, Quon H et al. Diffusion-weighted magnetic resonance imaging for predicting and detecting early response to chemoradiation therapy of squamous cell carcinomas of the head and neck. *Clinical Cancer Research* 2009;15:986-994.
- [49] Seppenwoolde Y, Engelsman M, De Jaeger K et al. Optimizing radiation treatment plans for lung cancer using lung perfusion information. *Radiother Oncol* 2002;63:165-177.
- [50] Brahme A. Biologically optimized 3-dimensional in vivo predictive assay-based radiation therapy using positron emission tomography-computerized tomography imaging. *Acta Oncol* 2003;42:123-136.
- [51] Madani I, Duthoy W, Derie C et al. Positron emission tomography-guided, focal-dose escalation using intensity-modulated radiotherapy for head and neck cancer. *Int J Radiat Oncol Biol Phys* 2007;68:126-135.
- [52] Yaremko BP, Guerrero TM, Noyola-Martinez J et al. Reduction of normal lung irradiation in locally advanced non small cell lung cancer patients using ventilation images for functional avoidance. *Int J Radiat Oncol Biol Phys* 2007;68:562-571.
- [53] Feng M, Kong F, Gross M, Fernando S, Hayman JA, Ten Haken RK. Using fluorodeoxyglucose positron emission tomography to assess tumor volume during radiotherapy for non-small-cell lung cancer and its potential impact on adaptive dose escalation and normal tissue sparing. *Int J Radiat Oncol Biol Phys* 2009;73:1228-1234.
- [54] Tyagi N, Riaz N, Hunt M et al. Weekly response assessment of involved lymph nodes to radiotherapy using diffusion-weighted MRI in oropharynx squamous cell carcinoma. *Med Phys* 2016;43:137-147.
- [55] Wahl RL, Herman JM, Ford E. The Promise and pitfalls of positron emission tomography and single-photon emission computed tomography molecular imaging-guided radiation therapy. *Semin Radiat Oncol* 2011;21:88-100.
- [56] van der Heide UA, Houweling AC, Groenendaal G, Beets-Tan RGH, Lambin P. Functional MRI for radiotherapy dose painting. *Magn Reson Imaging* 2012;30:1216-1223.
- [57] Lagerwaard FJ, Haasbeek CJA, Smit EF, Slotman BJ, Senan S. Outcomes of risk-adapted fractionated stereotactic radiotherapy for stage I non-small-cell lung cancer. *Int J Radiat Oncol Biol Phys* 2008;70:685-692.
- [58] Warren S, Partridge M, Carrington R, Hurt C, Crosby T, Hawkins MA. Radiobiological determination of dose escalation and normal tissue toxicity in definitive

## REFERENCES

---

- chemoradiation therapy for esophageal cancer. *Int J Radiat Oncol Biol Phys* 2014;90:423-429.
- [59] Valdés Olmos RA, Keus RB, Takes RP et al. Scintigraphic assessment of salivary function and excretion response in radiation-induced injury of the major salivary glands. *Cancer* 1994;73:2886-2893.
- [60] Eisbruch A, Ten Haken RK, Kim HM, Marsh LH, Ship JA. Dose, volume, and function relationships in parotid salivary glands following conformal and intensity-modulated irradiation of head and neck cancer. *Int J Radiat Oncol Biol Phys* 1999;45:577-587.
- [61] Van Acker, F., Flamen P, Lambin P et al. The utility of SPECT in determining the relationship between radiation dose and salivary gland dysfunction after radiotherapy. *Nucl Med Commun* 2001;22:225-231.
- [62] Buus S, Grau C, Munk OL, Bender D, Jensen K, Keiding S. 11C-methionine PET, a novel method for measuring regional salivary gland function after radiotherapy of head and neck cancer. *Radiother Oncol* 2004;73:289-296.
- [63] Astreinidou E, Roesink JM, Raaijmakers CPJ et al. 3D MR Sialography as a tool to investigate radiation-induced xerostomia: Feasibility study. *Int J Radiat Oncol Biol Phys* 2007;68:1310-1319.
- [64] Dirix P, De Keyzer F, Vandecaveye V, Stroobants S, Hermans R, Nuyts S. Diffusion-weighted magnetic resonance imaging to evaluate major salivary gland function before and after radiotherapy. *Int J Radiat Oncol Biol Phys* 2008;71:1365-1371.
- [65] Clark HD, Moiseenko VV, Rackley TP, Thomas SD, Wu JS, Reinsberg SA. Development of a method for functional aspect identification in parotid using dynamic contrast-enhanced magnetic resonance imaging and concurrent stimulation. *Acta Oncol* 2015;54:1686-1690.
- [66] Pos F, Bex A, Dees-Ribbers HM, Betgen A, van Herk M, Remeijer P. Lipiodol injection for target volume delineation and image guidance during radiotherapy for bladder cancer. *Radiother Oncol* 2009;93:364-367.
- [67] Chai X, van Herk M, van de Kamer JB et al. Behavior of lipiodol markers during image guided radiotherapy of bladder cancer. *Int J Radiat Oncol Biol Phys* 2010;77:309-314.

- [68] Tenhunen M, Collan J, Kouri M et al. Scintigraphy in prediction of the salivary gland function after gland-sparing intensity modulated radiation therapy for head and neck cancer. *Radiother Oncol* 2008;87:260-267.
- [69] Kapanen M. Accuracy of absorbed dose in external photon beam radiotherapy : what level is sufficient and how to approach it? PhD Thesis. University of Helsinki, Report Series in Physics. Helsinki University Print, Helsinki, Finland, 2009.
- [70] Hunter KU, Fernandes LL, Vineberg KA et al. Parotid glands dose–effect relationships based on their actually delivered doses: implications for adaptive replanning in radiation therapy of head-and-neck cancer. *Int J Radiat Oncol Biol Phys* 2013;87:676-682.
- [71] International Commission on Radiation Units and Measurements (ICRU). Prescribing, recording, and reporting photon-beam intensity-modulated radiation therapy (IMRT). *Journal of the ICRU* 2010; Report 83.
- [72] Turner SL, Swindell R, Bowl N et al. Bladder movement during radiation therapy for bladder cancer: Implications for treatment planning. *Int J Radiat Oncol Biol Phys* 1997;39:355-360.
- [73] Mangar SA, Scurr E, Huddart RA et al. Assessing intra-fractional bladder motion using cine-MRI as initial methodology for Predictive Organ Localization (POLO) in radiotherapy for bladder cancer. *Radiother Oncol* 2007;85:207-214.
- [74] Muren LP, Redpath AT, Lord H, McLaren D. Image-guided radiotherapy of bladder cancer: Bladder volume variation and its relation to margins. *Radiother Oncol* 2007;84:307-313.
- [75] Yee D, Parliament M, Rathee S, Ghosh S, Ko L, Murray B. Cone beam CT imaging analysis of interfractional variations in bladder volume and position during radiotherapy for bladder cancer. *Int J Radiat Oncol Biol Phys* 2010;76:1045-1053.
- [76] Dees-Ribbers H, Betgen A, Pos FJ, Witteveen T, Remeijer P, van Herk M. Inter- and intra-fractional bladder motion during radiotherapy for bladder cancer: A comparison of full and empty bladders. *Radiother Oncol* 2014;113:254-259.
- [77] Nicolle LE. Catheter associated urinary tract infections. *Antimicrobial Resistance and Infection Control* 2014;3:1-8.
- [78] Lotz HT, van Herk M, Betgen A, Pos F, Lebesque JV, Remeijer P. Reproducibility of the bladder shape and bladder shape changes during filling. *Med Phys* 2005;32:2590-2597.

## REFERENCES

---

- [79] Grønborg C, Vestergaard A, Høyer M et al. Intra-fractional bladder motion and margins in adaptive radiotherapy for urinary bladder cancer. *Acta Oncol* 2015;54:1461-1466.
- [80] Foroudi F, Pham D, Bressel M, Gill S, Kron T. Intrafraction bladder motion in radiation therapy estimated from pretreatment and posttreatment volumetric imaging. *Int J Radiat Oncol Biol Phys* 2013;86:77-82.
- [81] Lalondrelle S, Huddart R, Warren-Oseni K et al. Adaptive-predictive organ localization using cone-beam computed tomography for improved accuracy in external beam radiotherapy for bladder cancer. *Int J Radiat Oncol Biol Phys* 2011;79:705-712.
- [82] Yan D, Jaffray DA, Wong JW. A model to accumulate fractionated dose in a deforming organ. *Int J Radiat Oncol Biol Phys* 1999;44:665-675.
- [83] Lutkenhaus LJ, Visser J, de Jong R, Hulshof MCCM, Bel A. Evaluation of delivered dose for a clinical daily adaptive plan selection strategy for bladder cancer radiotherapy. *Radiother Oncol* 2015;116:51-56.
- [84] Vestergaard A. On-line adaptive radiotherapy for urinary bladder cancer to account for anatomical changes. PhD dissertation. Health, Aarhus University, Aarhus, Denmark 2015.
- [85] Gill S, Pham D, Dang K et al. Plan of the day selection for online image-guided adaptive post-prostatectomy radiotherapy. *Radiother Oncol* 2013;107:165-170.
- [86] Lutkenhaus LJ, de Jong R, Geijsen ED, Visser J, van Wieringen N, Bel A. Potential dosimetric benefit of an adaptive plan selection strategy for short-course radiotherapy in rectal cancer patients. *Radiother Oncol* 2016;119:525-30.
- [87] Bussels B, Maes A, Flamen P et al. Dose–response relationships within the parotid gland after radiotherapy for head and neck cancer. *Radiother Oncol* 2004;73:297-306.
- [88] Blanco AI, Chao KSC, El Naqa I et al. Dose–volume modeling of salivary function in patients with head-and-neck cancer receiving radiotherapy. *Int J Radiat Oncol Biol Phys* 2005;62:1055-1069.
- [89] Houweling AC, Philippens MEP, Dijkema T et al. A comparison of dose–response models for the parotid gland in a large group of head-and-neck cancer patients. *Int J Radiat Oncol Biol Phys* 2010;76:1259-1265.
- [90] Beetz I, Schilstra C, Burlage FR et al. Development of NTCP models for head and neck cancer patients treated with three-dimensional conformal radiotherapy for

xerostomia and sticky saliva: The role of dosimetric and clinical factors. *Radiother Oncol* 2012;105:86-93.

[91] Clark H, Hovan A, Moiseenko V, Thomas S, Wu J, Reinsberg S. Regional radiation dose susceptibility within the parotid gland: Effects on salivary loss and recovery. *Med Phys* 2015;42:2064-2071.

[92] Roesink JM, Moerland MA, Battermann JJ, Hordijk GJ, Terhaard CHJ. Quantitative dose-volume response analysis of changes in parotid gland function after radiotherapy in the head-and-neck region. *Int J Radiat Oncol Biol Phys* 2001;51:938-946.

[93] Firat F, Cermik TF, Sarikaya A, Berkarda S. Effects of gender and age on the quantitative parameters of [99mTc]pertechnetate salivary gland scintigraphy in normal subjects. *Nucl Med Commun* 2006;27:447-453.

[94] Castadot P, Geets X, Lee JA, Christian N, Gregoire V. Assessment by a deformable registration method of the volumetric and positional changes of target volumes and organs at risk in pharyngo-laryngeal tumors treated with concomitant chemo-radiation. *Radiother Oncol* 2010;95:209-217.